

Extended Dynamical Mean Field Theory and GW method

Ping Sun and Gabriel Kotliar

Center for Materials Theory, Department of Physics and Astronomy, Rutgers University,

Piscataway, NJ 08854-8019

(October 30, 2018)

Abstract

We develop the extended dynamical mean field theory (E-DMFT) with a view towards realistic applications. **1)** We introduce an intuitive derivation of the E-DMFT formalism. By identifying the Hartree contributions before the E-DMFT treatment, it allows to handle systems in symmetry breaking phases within a simple formalism. **2)** We make a new implementation of E-DMFT through real Hubbard-Stratonovich transformation to decouple the non-local two-particle interactions. We apply it to a 3D U-V model, with U the on-site and V the nearest neighbor interactions, and investigate the behavior of the various Green's functions, especially the density susceptibility, as the density instability is approached. We obtain the phase diagram at a finite temperature. **3)** We present a formalism incorporating E-DMFT with Cellular DMFT. **4)** We suggest an improvement of the E-DMFT approach by combining it with a generalized GW method. The method combines the local self-energy from E-DMFT and the non-local ones from the perturbative calculation of GW. We apply the method to a 1D U-V model with two sublattices carrying different chemical potentials. By comparing with those from Density Matrix Renormalization Group (DMRG) calculations, we show the results are shifted in the correct direction due to the GW contributions. **5)** In order to handle the generic Coulomb repulsion within E-DMFT, we describe

a method to tailor E-DMFT so that proper momentum dependence can be kept in general response functions.

71.10.-w, 71.30.+h

I. INTRODUCTION

The Dynamical Mean Field Theory (DMFT) has been a powerful tool for the study of strongly correlated electronic systems. It has allowed us to gain new insights into non-perturbative problems such as the Mott paramagnetic metal to paramagnetic insulator transition at finite temperatures¹. There are many current attempts to extend the scope of the DMFT approach in several directions: to include momentum dependence in the self-energy¹⁻⁷, to account for the effects of finite range interactions⁸⁻¹⁴, and to combine DMFT with realistic band structure¹⁵⁻¹⁸.

The current paper is devoted to the investigation of the Extended Dynamical Mean Field Theory (E-DMFT), an extension of the original DMFT in order to take into account the spatially non-local interactions beyond the Hartree level. The idea of E-DMFT was developed independently in the studies of spin glass^{8,11}, systems with non-local Coulomb interaction^{9,12}, and the heavy fermion system¹⁰. The derivation of E-DMFT based on Baym-Kadanoff functional has been achieved in Ref.[¹²].

We present here several methodological developments which build on the E-DMFT approach with a view to obtain a more realistic description of solids. Our goals are to describe **a)** the frequency dependence of the effective interaction and its effects on the single particle spectra, **b)** the effects of short range correlations, and **c)** a momentum dependent polarization. These three effects certainly present in realistic models of solids¹⁹⁻²². We discuss them in this paper in the framework of model Hamiltonians in sections IV, VII, and VIII. It should be pointed out that the problem is not touched in this paper as how to obtain the parameters of the model Hamiltonian from the first principle calculations.

In addition we present several technical advances for the analysis of E-DMFT equations. In sections II and III, we present a simplified derivation of these equations in a broken

symmetry phase. A method for handling arbitrary interactions within E-DMFT-QMC by an interaction shift²³ is also discussed in the section. We show the formalism combining E-DMFT with cellular DMFT (C-DMFT) in §V and with GW approximation²⁴ in §VI.

To illustrate the ideas and the working of the methods we apply them to two problems. The transitions between a Mott insulator (MI), a band insulator (BI), and a Fermi liquid (FL) in a 3D U-V model is discussed in §IV. The model describes an electron system with an on-site repulsion U and a nearest neighbor interaction V. It was treated in simple DMFT at half² and quarter²⁵ fillings and is relevant to the materials with charge ordered phase^{26–28}. The problem of the transition between MI and BI phases in a 1D U-V model with alternating chemical potential was discussed in the context of mixed stack organic compounds^{29,30} and ferroelectric perovskites³¹. We exhibit in §VII the implementation of E-DMFT-GW method on the 1D model. §IX is the conclusion.

II. MODEL HAMILTONIAN

We start with the following Hamiltonian:

$$\begin{aligned} \hat{H} = & -\frac{1}{2} \sum_{i,j} \sum_{\sigma} (t_{ij} \hat{c}_{i\sigma}^{\dagger} \hat{c}_{j\sigma} + \text{h.c.}) - \sum_i \sum_{\alpha=0}^3 h_{i\alpha} \hat{S}_{i\alpha} \\ & + U \sum_i \hat{n}_{i\uparrow} \hat{n}_{i\downarrow} + \frac{1}{2} \sum_{i,j} \sum_{\alpha,\beta=0}^3 \hat{S}_{i\alpha} V_{i\alpha,j\beta} \hat{S}_{j\beta}. \end{aligned} \quad (1)$$

The operators $\hat{S}_{i\alpha} \stackrel{\text{def}}{=} \hat{c}_{i\sigma}^{\dagger} \tau_{\sigma,\sigma'}^{\alpha} \hat{c}_{i\sigma'}$ with τ^{α} being the Pauli matrices for $\alpha = 1, 2, 3$ and $\tau^0 = I_{2 \times 2}$, the identity. So the zero-th component of $\hat{S}_{i\alpha}$ is the charge density and the rest the spin operators. Similarly, $h_{i\alpha=0}$ represents the chemical potential and the other three, with $\alpha = 1, 2, 3$, the external magnetic field.

In Eq.(1) the on-site part of the interaction is isolated in U and the off-site parts are described by $V_{i\alpha,j\beta}$, hence $V_{i\alpha,i\beta} = 0$. We have allowed all the possible forms of the instantaneous direct and exchange interactions, but excluded some others, like the pair hoppings. Unless otherwise specified, the form of the interaction $V_{i\alpha,j\beta}$ will be generic with only the simple requirements that the interaction be translational invariant, $V_{i\alpha,j\beta} = V_{\alpha,\beta}(|i - j|)$, and symmetric, $V_{i\alpha,j\beta} = V_{j\beta,i\alpha}$. Due to the possible ionic screening and the super-exchange mechanisms, we have the freedom to certain extent in choosing U and the components of V independently at the level of the model Hamiltonian. While it is reasonable to take $U > 0$, in the off-site interaction matrix V all possibilities are allowed if some effective forms of the interactions are under consideration. In other words, the matrix V is not necessarily positive- or negative- definite.

In this paper we keep for simplicity $h_0, h_3 \neq 0$ and set $h_1, h_2 = 0$. This choice is more general than it appears since we can always choose the direction of the effective magnetic field to be the z-direction by appropriately rotating the system. Furthermore, we assume that the spin symmetry breaking, if it may happen, is also along the z-direction. This assumption is very natural if $V_{i\alpha,j\beta}$ is symmetric under the permutation among the three directions. However, it is actually more restrictive since it requires that if $V_{\alpha,\beta}(|i - j|)$ produces any easy-axis, the direction of the easy-axis should be also in the z-direction. We can then define a spin-dependent chemical potential:

$$\mu_{i\sigma} \stackrel{\text{def}}{=} h_{i0} + \sigma h_{i3}$$

Before deriving the E-DMFT formalism, we need first to separate out the Hartree contributions from the interactions. It is known from the Baym-Kadanoff functional analysis of E-DMFT¹² that in the phases with broken symmetry, Hartree terms contribute to the E-DMFT by shifting the chemical potential³². In the current case, due to the spin exchanges, this shift is spin-dependent. It is also known that in the circumstance of C-DMFT³³, one needs to handle separately the Hartree contributions from the non-local interaction across

the cluster boundary. With all these motivations, we rewrite the Hamiltonian as follows:

$$\begin{aligned} \hat{H} = & -\frac{1}{2} \sum_{i,j} \sum_{\sigma} (t_{ij} \hat{c}_{i\sigma}^{\dagger} \hat{c}_{j\sigma} + \text{h.c.}) - \sum_{i,\sigma} \mu_{i\sigma}^{\text{eff}} n_{i\sigma} \\ & + U \sum_i : \hat{n}_{i\uparrow} :: \hat{n}_{i\downarrow} : + \frac{1}{2} \sum_{i \neq j} \sum_{\alpha,\beta=0}^3 : \hat{S}_{i\alpha} : V_{i\alpha,j\beta} : \hat{S}_{j\beta} : \end{aligned} \quad (2)$$

where the normal ordering of the operators is defined by $: \mathcal{O} \stackrel{\text{def}}{=} \mathcal{O} - \langle \mathcal{O} \rangle$ with the average over the ground state. The effective chemical potential is defined to be

$$\mu_{i\sigma}^{\text{eff}} = \mu_{i\sigma} - \frac{1}{2} U - \sum_{j(\neq i)} V_{i0,j0} (\langle n_{j\uparrow} \rangle + \langle n_{j\downarrow} \rangle) - \sigma \sum_{j(\neq i)} V_{i3,j3} (\langle n_{j\uparrow} \rangle - \langle n_{j\downarrow} \rangle) \quad (3)$$

We work with the functional integral representation of the partition function at finite temperature $0 < T = 1/\beta < \infty$ ³⁴. We want to perform a Hubbard-Stratonovich transform and decouple the V -interactions⁴. Since ultimately we will map the many-body system to an impurity model and solve the self-consistent impurity problem via numerical techniques like QMC, it is desired that the Hubbard-Stratonovich transform be real²³. To this end, we need first to add the identity matrices $\lambda_{\alpha\beta} \mathbf{I}_{ij}$ to the off-site interaction to ensure that, for given α and β , the matrix

$$[\tilde{V}_{\alpha\beta}]_{ij} \stackrel{\text{def}}{=} \lambda_{\alpha\beta} \mathbf{I}_{ij} - [V_{\alpha\beta}]_{ij} \quad (4)$$

is positive-definite. The minus sign in front of the bare interaction in the above equation is needed for a real Hubbard-Stratonovich transform. Practically we can take any value of $\lambda_{\alpha\beta}$ as long as it is greater than the biggest eigen value of the matrix $[V_{\alpha\beta}]$ whose elements are defined by $[V_{\alpha\beta}]_{ij} \stackrel{\text{def}}{=} V_{i\alpha,j\beta}$. To keep the symmetry, we require $\lambda_{\alpha\beta} = \lambda_{\beta\alpha}$. Using Hubbard-Stratonovich transform, one can write the partition function in terms of the following functional integral:

$$Z = \int \mathcal{D}[c_{i,\sigma}^{\dagger}(\tau), c_{i,\sigma}(\tau); \phi_{i,\alpha}(\tau)] \exp(-S) \quad (5)$$

with the Euclidean action:

$$\begin{aligned}
S = & \int_0^\beta d\tau \left\{ \sum_{i,\sigma} c_{i\sigma}^\dagger(\tau) \partial_\tau c_{i\sigma}(\tau) - \sum_{i,j} \sum_\sigma [t_{ij} c_{i\sigma}^\dagger(\tau) c_{j\sigma}(\tau) + \text{h.c.}] - \sum_{i,\sigma} \mu_{i,\sigma}^{\text{eff}} n_{i,\sigma} \right. \\
& \left. + U^{\text{eff}} \sum_i : n_{i\uparrow}(\tau) :: n_{i\downarrow}(\tau) : + \frac{1}{2} \sum_{i,j} \sum_{\alpha,\beta=0}^3 \phi_{i\alpha}(\tau) [\tilde{V}_{\alpha\beta}]_{ij}^{-1} \phi_{j,\beta}(\tau) \pm \sum_i \sum_{\alpha=0}^3 \phi_{i\alpha}(\tau) : S_{i\alpha}(\tau) : \right\}, \quad (6)
\end{aligned}$$

where

$$U^{\text{eff}} = U + \tilde{V}_{i0,i0} - \tilde{V}_{i1,i1} - \tilde{V}_{i2,i2} - \tilde{V}_{i3,i3} = U + \lambda_{00} - \lambda_{11} - \lambda_{22} - \lambda_{33}$$

While the λ dependences are explicitly contained in the effective on-site interaction U^{eff} and the interaction matrices $\tilde{V}_{\alpha\beta}$, they cancel each other exactly so that all the physically measurable quantities are independent of λ . The electron-phonon vertex defined in Eq.(6) is local. In an insulator with a long range Coulomb interaction, one needs a different choice of the vertex, as will be discussed later in §VIII.

Several remarks are in place. First, since our strategy is to separate out all the Hartree contributions from the interactions, we certainly need to treat the auxiliary field in the same way. However, due to the identity

$$\langle \phi_{i\alpha} \rangle = \mp \sum_j \sum_{\beta=0}^3 [\tilde{V}_{\alpha\beta}]_{ij} \langle : S_{j\beta} : \rangle = 0,$$

we need not bother to normal order the ϕ fields here. The current formalism of E-DMFT can be extended directly to a general bose field¹³ which can develop non-zero expectation values, if we replace $\phi_{i\alpha}$ by $: \phi_{i\alpha} :$. Second, there is an arbitrariness in choosing the sign of the electron-phonon vertex which is reflected in the “ \pm ” signs appeared in Eq.(6). It comes from the freedom in the Ising (Z_2) symmetry of the order parameters. For definiteness, we take ‘ $-$ ’ from now on. Finally, one can also try to decouple the on-site interaction by using yet another continuous auxiliary field. Because this interaction does not get any renormalization as we derive the E-DMFT, and because for the local density-density interaction there is the more efficient Hirsch-Fye algorithm³⁵ which uses the discrete Ising auxiliary field, we will not implement this here³⁶.

For future reference, we first define the following Matsubara Green's function:

$$G_{i\sigma,j\sigma'}(\tau - \tau') \stackrel{\text{def}}{=} -\langle T_\tau c_{i\sigma}(\tau) c_{j\sigma'}^\dagger(\tau') \rangle, \quad (7)$$

$$\chi_{i\alpha,j\beta}(\tau - \tau') \stackrel{\text{def}}{=} -\langle T_\tau : S_{i\alpha}(\tau) :: S_{j\beta}(\tau') : \rangle, \quad (8)$$

$$D_{i\alpha,j\beta}(\tau - \tau') \stackrel{\text{def}}{=} -\langle T_\tau : \phi_{i\alpha}(\tau) :: \phi_{j\beta}(\tau') : \rangle. \quad (9)$$

Notice that the auxiliary field Green's function D depends on the value of λ introduced to make the effective interaction matrix \tilde{V} positive definite while the Green's functions for the electrons do not. The auxiliary phonon Green's functions are related to the electronic two-particle response functions by the following identity, which can be derived by integrating out the auxiliary degrees of freedom in the phonon Green's function,

$$\chi^{-1}(k, i\omega_n) = \tilde{V}_k + \Pi^{-1}(k, i\omega_n) \quad (10)$$

with the self-energy given by the Dyson equation for the phonons:

$$\Pi(k, i\omega_n) = -\tilde{V}_k^{-1} - D^{-1}(k, i\omega_n), \quad (11)$$

where $\omega_n = (2\pi/\beta)n$ for integer n . The above two equations are in the matrix form in the charge-spin space labeled by $\alpha = 0, 1, 2, 3$. The bare interaction vertex $-\tilde{V}_k$ plays the role as the free propagator and is defined as $[\tilde{V}_k]_{\alpha\beta} \stackrel{\text{def}}{=} (1/L^d) \sum_{j,l} \tilde{V}_{j\alpha,l\beta} \exp[-ik \cdot (j - l)]$. For later use, we also write down the Dyson equation for the electron Green's function:

$$\Sigma(k, ip_n) = ip_n - t_k - G^{-1}(k, ip_n). \quad (12)$$

with $p_n = (2\pi/\beta)(n + 1/2)$ for integer n . The equation is in the 2×2 matrix form labeled by the spin $\sigma = \uparrow, \downarrow$.

With the above preparation, we now derive E-DMFT. We will consider two situations. In the next section we describe the first case, the E-DMFT for a homogeneous system in

which all the lattice sites are equivalent to each other. In this case E-DMFT approximation amounts to integrating out all but one lattice site to get an effective single site action which is equivalent to a self-consistent impurity model. All the sites that are integrated out contribute to self-consistent baths of free fermions and bosons for the impurity model. Here we should have a homogeneous chemical potential $\mu_{i\sigma} = \mu_\sigma$. In the second case (see §V) we explore the E-DMFT for systems with two mutually penetrating sublattices. We present a formalism combining E-DMFT and C-DMFT with a cluster of two neighboring sites. While it is natural to apply this formalism to a system with two non-equivalent sublattices, it can also be applied to the homogeneous situation. In the latter case, the purpose is to treat more accurately the spatial correlations than the single site E-DMFT. This combination of E-DMFT and C-DMFT can be formulated for clusters of arbitrary size.

III. E-DMFT OF A HOMOGENEOUS SYSTEM

We first explore the single site E-DMFT applicable to a homogeneous system. By keeping one lattice site while integrating out the rest using the cavity construction¹, we obtain the E-DMFT effective action³²

$$\begin{aligned}
S_0^{\text{eff}} = & - \int_0^\beta d\tau \int_0^\beta d\tau' \sum_\sigma c_{0,\sigma}^\dagger(\tau) \mathcal{G}_\sigma^{-1}(\tau - \tau') c_{0,\sigma}(\tau') \\
& - \frac{1}{2} \int_0^\beta d\tau \int_0^\beta d\tau' \sum_{\alpha,\beta=0}^3 : \phi_{0\alpha}(\tau) : \mathcal{D}_{\alpha\beta}^{-1}(\tau - \tau') : \phi_{0\beta}(\tau') : \\
& + U^{\text{eff}} \int_0^\beta d\tau : n_{0,\uparrow}(\tau) :: n_{0,\downarrow}(\tau) : - \int_0^\beta d\tau \sum_{\alpha=0}^3 : \phi_{0\alpha}(\tau) :: S_{0,\alpha}(\tau) :
\end{aligned} \tag{13}$$

This is an impurity model with both electron and (auxiliary) phonon degrees of freedom. The impurity model Green's functions are identified with the local Green's functions of the lattice model, namely [see Eqs.(7)-(9)],

$$G_{\sigma\sigma'}^{\text{loc}}(\tau - \tau') = G_{0\sigma,0\sigma'}(\tau - \tau'), \quad \chi_{\alpha\beta}^{\text{loc}}(\tau - \tau') = \chi_{0\alpha,0\beta}(\tau - \tau'), \quad D_{\alpha\beta}^{\text{loc}}(\tau - \tau') = D_{0\alpha,0\beta}(\tau - \tau'). \quad (14)$$

The E-DMFT self-consistent loop is formed as follows. One starts with the effective action Eq.(13) and measures the local electron and phonon Green's functions as define through Eq.(14). Then one calculates the self-energies using the local version of the Dyson equations:

$$\Sigma_{\sigma}(ip_n) = \mathcal{G}_{\sigma}^{-1}(ip_n) - [G_{\sigma}^{\text{loc}}]^{-1}(ip_n), \quad (15)$$

$$\Pi(i\omega_n) = \mathcal{D}^{-1}(i\omega_n) - [D^{\text{loc}}]^{-1}(i\omega_n) \quad (16)$$

One of the basic assumptions of DMFT is the locality of the self-energy¹. Notice that from Eq.(10) the phonon self-energy is different from, although related to, the response functions and the locality of the former does not imply the locality of the latter. Under this assumption, the same local quantities can be calculated, by using Eqs. (10)-(12),

$$G_{\sigma}^{\text{loc}}(ip_n) = \sum_k G_{\sigma}(k, ip_n) = \sum_k [ip_n - t_k - \mu_{\sigma}^{\text{eff}} - \Sigma_{\sigma}(ip_n)]^{-1}, \quad (17)$$

$$\chi^{\text{loc}}(i\omega_n) = \sum_k \chi(k, i\omega_n) = \sum_k [\tilde{V}_k + \Pi^{-1}(i\omega_n)]^{-1}, \quad (18)$$

$$D^{\text{loc}}(i\omega_n) = \sum_k D(k, i\omega_n) = - \sum_k [\tilde{V}_k^{-1} + \Pi(i\omega_n)]^{-1} \quad (19)$$

In the DMFT with phonons¹³, one substitutes the results of Eqs.(17) and (19) back in the local Dyson equations, (15) and (16), and generates a new set of the Dynamical Weiss functions \mathcal{G} and \mathcal{D} which serve as the starting point of the next iteration. This completes the self-consistent loop.

It is interesting to notice, however, that one has another choice to form the self-consistent loop through the electronic two particle Green's function χ^{loc} instead of D^{loc} , as used in Refs.[^{9,10,12}]. It is important that the two different procedures are compatible with each

other. By combining Eqs.(18) and (19), one can find the following relation in the matrix form:

$$[\chi^{\text{loc}}]^{-1}(i\omega_n) = -\mathcal{D}(i\omega_n) + \Pi^{-1}(i\omega_n) \quad (20)$$

where the local phonon Dyson equation (16) has been used. This is nothing but the identity one can derive directly from the effective action Eq.(13) and is the local version of the electron-phonon identity, Eq.(10). Hence the two routines, which correspond to making the DMFT approximation at the different stages of the formulation, one directly from the non-local electron interaction and the other after the Hubbard-Stratonovich decomposition, are indeed equivalent, as long as the same interaction vertex defined in Eq.(4) is used.

There is, though, still one point left out, that is the arbitrariness of the value of the constants $\lambda_{\alpha\beta}$ in Eq.(4). They were introduced in our formalism for the purpose of ensuring the applicability of the real Hubbard-Stratonovich transform and are thus unphysical. While it is obvious that the artificial effects from the λ dependences cancel out exactly in the original action, Eq.(6), it is not clear if the same thing happens after the E-DMFT approximation. On the other hand, the earlier versions of E-DMFT^{9,10,12} use only the bare interactions and have no such a problem.

We will show in the following that, even after the E-DMFT approximation, the effects from these λ terms still cancel exactly in *all* measurable quantities and only the physical interactions determine the physics. In doing so, we also establish the equivalence of our E-DMFT with the existing ones. The physical reason behind this perfect cancellation is that the static quartic interactions, including the λ terms we introduced, do not get any renormalization in DMFT, even in the presence of those non-local interactions.

To proceed, we need to check the effects on the phonon dynamical Weiss functions of the arbitrary λ dependence we added in Eq.(4) for ensuring the positive-definiteness. These

are easily seen by checking the high frequency behavior of the phonon Weiss functions. In this limit, the phonon self-energy goes to zero at the rate of the inverse frequency square, since it is approximately proportional to the local two particle Green's function as shown in Eq.(20) (remember \mathcal{D} approaches a finite constant in the same limit). So from Eq.(19) we have:

$$D_{\alpha\beta}^{\text{loc}}(i\omega_n) \xrightarrow{n \rightarrow \infty} -\sum_k \tilde{V}_{k,\alpha\beta} = -\lambda_{\alpha\beta} \quad (21)$$

and thus

$$\mathcal{D}_{\alpha\beta}(i\omega_n) \xrightarrow{n \rightarrow \infty} -\lambda_{\alpha\beta} \quad (22)$$

We can make a shift of the dynamical phonon Weiss functions by defining (in the matrix form)

$$\tilde{\mathcal{D}}(i\omega_n) \stackrel{\text{def}}{=} \mathcal{D}(i\omega_n) + \lambda \quad (23)$$

The Weiss function defined above approaches zero in the high frequency limit. We then integrate out the auxiliary fields in the effective action Eq.(13). After rearranging the variables and introducing a new set of the auxiliary field $\tilde{\phi}_{0,\alpha}$, the effective action becomes:

$$\begin{aligned} \tilde{S}_0^{\text{eff}} = & -\int_0^\beta d\tau \int_0^\beta d\tau' \sum_{\sigma\sigma'} c_{0,\sigma}^\dagger(\tau) \mathcal{G}_{\sigma\sigma'}^{-1}(\tau - \tau') c_{0,\sigma'}(\tau') - \frac{1}{2} \int_0^\beta d\tau \int_0^\beta d\tau' \sum_{\alpha,\beta=0}^3 \\ & : \tilde{\phi}_{0\alpha}(\tau) : \tilde{\mathcal{D}}_{\alpha\beta}^{-1}(\tau - \tau') : \tilde{\phi}_{0\beta}(\tau') : + U \int_0^\beta d\tau : n_{0,\uparrow}(\tau) : : n_{0,\downarrow}(\tau) : - \int_0^\beta d\tau \sum_{\alpha=0}^3 : \tilde{\phi}_{0\alpha}(\tau) : : S_{0,\alpha}(\tau) : \end{aligned} \quad (24)$$

It can be shown that, while the electronic Green's functions remain the same, the new local phonon Green's function \tilde{D}^{loc} is related to the old one by

$$\tilde{D}^{\text{loc}}(i\omega_n) = D^{\text{loc}}(i\omega_n) + \lambda + [\lambda + \mathcal{D}(i\omega_n)] \chi^{\text{loc}}(i\omega_n) [\lambda + \mathcal{D}(i\omega_n)] - \mathcal{D}(i\omega_n) \chi^{\text{loc}}(i\omega_n) \mathcal{D}(i\omega_n) \quad (25)$$

One can also find the relation between the phonon self-energies:

$$\tilde{\Pi}^{-1}(i\omega_n) = \Pi^{-1}(i\omega_n) + \lambda. \quad (26)$$

The self-consistent conditions, Eqs.(18) and (19), are transformed to

$$\tilde{\chi}^{\text{loc}}(i\omega_n) = \sum_k [-V_k + \tilde{\Pi}^{-1}(i\omega_n)]^{-1}, \quad (27)$$

$$\tilde{D}^{\text{loc}}(i\omega_n) = - \sum_k [-V_k^{-1} + \tilde{\Pi}(i\omega_n)]^{-1}. \quad (28)$$

The self-consistent loop can be formed in the same way as before.

So we have shown that the arbitrariness in the choice of λ does not affect the physical quantities. This point is best seen through Eq.(27) where a simultaneous shift of V_k and $\tilde{\Pi}^{-1}$ cancels out exactly. The quantities related to the auxiliary fields, including those described in Eqs. (23), (25), (26), and (28), do depend on λ . But as we pointed out, they are not quantities experimentally measurable.

The formalism shown above, Eqs.(24)-(28), is equivalent to, although more generic than, those discussed in the existing literatures, due to (i) the more general form of the interaction we have taken, (ii) the consideration paid to possible broken symmetry, and (iii) the introduction of the λ terms ensuring the positive-definiteness of the interaction matrix. The method allows us to study the models with general interactions, like the antiferromagnetic spin exchange.

Before we leave this part, it should be pointed out that the formalism we just developed can readily be applied to the general case containing electron-phonon and long range Coulomb interactions. There is basically only one change needed. Due to the dynamics of the real phonons from themselves, we have an additional term $(i\omega_n)^2$ in those related equations, including (10), (11), (18), (19), and (28). The electron-phonon identities still hold in the new formalism. Without any further change, the continuous auxiliary boson fields can

be used to describe the real phonon fields within the same formalism.

IV. APPLICATION I: PHASE DIAGRAM OF THE 3D U-V MODEL AT HALF-FILLING VIA E-DMFT

As an example of the practical implementation, in the following we apply the E-DMFT formalism based on the continuous auxiliary field approach to a 3D Hubbard model with a nearest neighbor density-density repulsion (the U-V model). We will be interested in the case at half-filling. This is a much simplified version of the model we have investigated in the last section. Especially, there is only one local shift, $\lambda = \lambda_{00}$, needed to make the interaction matrix positive-definite. Our purpose is to demonstrate the implementation of E-DMFT and investigate the behavior of the density response function in approaching the CDW phase transition. Under the given condition, this model Hamiltonian allows three different phases: the Mott insulating phase when U is dominant; the band insulating phase with CDW when V prevails; the metallic Fermi liquid phase when the kinetic energy overcomes the interactions. In the MI phase the system can develop an antiferromagnetic long order if the magnetic frustration is weak enough. For simplicity, in the following we will consider the system at a high enough temperature such that the MI phase is paramagnetic due to the strong thermal fluctuations. A finite temperature phase diagram at $\beta = 5.0$ is presented in Fig.1. In the temperature region where our study is performed, the Mott transition is actually a crossover¹ so the phase diagram in Fig.1 should be viewed as a qualitative representation of the actual phase diagram at $T = 0$.

The 3D U-V model allows us to illustrate the novel aspects of our methodology, including the implementation of E-DMFT with an auxiliary field, carrying out QMC simulation with repulsive interactions, cancellation of the λ dependence, and investigation of the density-density response. Physically, we have in mind the following questions: (1) How is the MI-FL

transition affected by the non-local interaction V ? (2) How does the charge density instability develop in the E-DMFT equations? (3) How does a frequency dependent effective interaction affect the quasiparticle properties? These questions can not be addressed in the simple DMFT studies where the V interaction is handled at the Hartree level.

The following is the 3D model Hamiltonian we are going to study:

$$\begin{aligned} \hat{H} = & -\frac{1}{2} \sum_{i,j} \sum_{\sigma} (t_{ij} \hat{c}_{i\sigma}^{\dagger} \hat{c}_{j\sigma} + \text{h.c.}) + U \sum_i : \hat{n}_{i\uparrow} :: \hat{n}_{i\downarrow} : \\ & + V \sum_{\langle i,j \rangle} (: \hat{n}_{i\uparrow} : + : \hat{n}_{i\downarrow} :) (: \hat{n}_{j\uparrow} : + : \hat{n}_{j\downarrow} :), \end{aligned} \quad (29)$$

where $\langle i, j \rangle$ represents a pair of nearest-neighboring sites. In this special case, the Fourier transformed off-site interaction is given by

$$V_k = V[\cos(k_x) + \cos(k_y) + \cos(k_z)]. \quad (30)$$

We perform QMC simulation similar to that in Ref.^[13]. The fermionic part of the impurity model is handled by the standard Hirsch-Fye algorithm³⁵. The statistical weight from the part of the continuous bosonic fields is obtained directly by computing the corresponding Boltzmann factor. We use here a semi-circular density of state for the electronic degrees of freedom¹³. The bandwidth is set to be the energy unit. We consider paramagnetic solutions at a finite temperature. Since the system is exactly at half-filling, we use in QMC the particle-hole symmetry accompanied by the reversal of the phonon displacement to increase the efficiency of the simulation. In QMC, we take $\beta = 5.0$ and $\Delta\tau = 1/4$. Correspondingly the inverse temperature range $[0, \beta]$ is divided into $L = \beta/\Delta\tau = 20$ slices. The typical number of sweeps for QMC measurement is 10^6 by which all the quantities converge within the statistical errors. We actually experience critical slowing down in both QMC simulation and the DMFT self-consistent iterations as we approach the critical point around $U = 3.0$ and $V = 1.6$ (see Fig.1). In this region the typical number of iterations needed for convergence increases from ten to twenty and we use in QMC measurement $2 \sim 4 \times 10^6$ sweeps.

Before we present the results, we want to show that at the numerical level, the λ depending term does not affect the physical results. We have shown in the previous section that in the formulation of E-DMFT the λ dependence does not show up in physical quantities. However it can happen that if the formalism is so sensitive to the dependence such that in a practical calculation like QMC there is always only partial cancellation and a significant λ dependence remains in the physical measurables. It is also possible that a negligible λ dependence in the results of the impurity model, which is always there unless one can solve the problem exactly, may get magnified during the E-DMFT iterations. In the following we present the results calculated at $U = 3.0$ and $V = 1.6$ which show no λ dependence. From the phase diagram Fig.1 one can see that this is the point we have reached closest in the parameter space to the finite temperature critical point (CP). If the suggested scenarios of the λ dependence in the physical results may happen, they most likely happen around the CP where the system becomes very sensitive to the extra change from λ . In Fig.2 we plot the imaginary part of the electron Green's functions calculated at four different λ 's. The result shows no λ dependence within the accuracy of the calculation³⁷. Similar for the electron density Green's functions as shown in Fig.3. So in both the formulation and the practical calculation, the λ term does not play any physical role and we can use it safely. In all the following calculation, we set $\lambda = 2.0$ in the QMC simulation.

A. Near the Mott Crossover Line

We first present the result showing the crossover between the MI and FL phases. In Fig.4 we show the data of $\text{Im } G_{\sigma}^{\text{loc}}(i\pi/\beta)$ v.s. U at $V = 0.0$ and 1.0 . The reason we choose to plot this function is that it is known¹ that the asymptotic behavior at the low frequency limit of the imaginary part of the electron Green's function reflects the density of states (DOS) near the Fermi surface. For the metallic phase the DOS is finite at the Fermi surface and hence $\text{Im } G(ip_n) \xrightarrow{p_n \rightarrow 0} \text{Const.} \neq 0$. For the insulating phase, on the other hand, the

corresponding DOS is zero and $\text{Im } G(ip_n) \xrightarrow{p_n \rightarrow 0} 0$. So from the plotting of $\text{Im } G$ at the first fermionic Matsubara frequency we can study the transition or crossover behavior between the two phases. Since we solve the problem at a temperature ($\beta = 5.0$) higher than the critical temperature ($\beta_c \sim 1/0.04$, see Ref.[1]) of the Mott transition, what we see in Fig.4 is that for fixed V , $-\text{Im } G_\sigma^{\text{loc}}(i\pi/\beta)$ decreases smoothly as U is increased. This behavior represents the crossover between the two phase. There is a small but finite shift in between the two curves calculated at $V = 0.0$ and 1.0 . This is a result of the competition between U and V . In the case of $V = 1.0$ the system enters the BI phase for $U \lesssim 2.2$ which one can see approximately from Fig.1. This region is out of the scope of the current approach applicable only to a homogeneous system. In the range $2.2 \lesssim U \lesssim 4.0$, which is, roughly speaking, the crossover region, the value of $\text{Im } G_\sigma^{\text{loc}}(i\pi/\beta)$ at the same U is always bigger for $V = 1.0$ than that for $V = 0.0$. This means that the existence of the finite V makes the system more metallic and so the effective U is smaller, as one anticipates from qualitative considerations. If U is increased further so that $4.0 \lesssim U$, both the systems enter the paramagnetic insulating phase with literally no difference.

We then investigate the behavior of the various Green's functions as the transition towards the band insulating phase is approached by changing V at fixed U . We first show the results at $U = 3.0$. We solve the problem for seven different values of the interaction: $V = 0.5, 1.0, 1.3, 1.4, 1.5, 1.6$, and 1.7 . In all the results presented below the data from the last case are not shown because we already encounter the instability at which the convergence of the self-consistent interaction is lost. So we can view $V = 1.7$ as an upper boundary of the metallic phase for $U = 3.0$. In Fig.5 we show the imaginary part of the electron Green's function and in Fig.6 the imaginary part of the electron self-energy. It can be seen clearly that, while the trends of the change of the plotted quantities are in the direction towards a more metallic phase as V is increased (that is, bigger $\text{Im}G$ and smaller self-energy at the first several Matsubara frequencies), the magnitudes of the changes are

very limited, especially in comparison with the phonon Green's functions³⁸ shown in Fig.7. The local phonon Green's function, which is related to the density susceptibility as we have shown in the last section, increases significantly as we approach the phase transition point. We can analyze the behavior from the self-consistent equation (19), which can be rewritten as

$$D^{\text{loc}}(i\omega_n) = \sum_k \frac{V_k}{1 - V_k \tilde{\Pi}(i\omega_n)}. \quad (31)$$

As a result of screening the phonon self-energy is negative. Moreover, $|\tilde{\Pi}(i\omega_n)|$ is a monotonically decreasing function of the frequency, since the screening becomes less effective as the frequency increases. Hence the instability, if it may happen, will first show up at the wave vector $k = q \stackrel{\text{def}}{=} (\pi, \pi, \pi)$ and the frequency $\omega_n = \omega_0 = 0$, where the product $V_q \tilde{\Pi}(i\omega_0) = -3V \tilde{\Pi}(i\omega_0)$ has the biggest positive value. In Fig.8 we show the plotting of $-3V \tilde{\Pi}(i\omega_0)$ v.s. V at the given U . The trend is obvious for the product to approach "1" where the corresponding denominator in Eq.(31) vanishes. This establishes the picture that as the transition point is approached, the denominator disappears first at q and ω_0 , which corresponds to an instability against the homogeneous ground state with a static CDW at wave vector (π, π, π) . This is a typical phenomenon in the Green's function description of phase transitions³⁹, although the quantities involved here are non-perturbative. The instability is signaled by a frequency of phonon becoming negative^{13,14}. At this point an ordered mean field state would be the correct solution. It should be noted that, even when the instability happens, one may still continue the paramagnetic solution of E-DMFT by taking the principle part in Eq.(31). But in 3D the convergence near transition is impossible because the derivative of the phonon Green's function with respect to the control parameter V becomes infinite.

B. Frequency Dependent On-Site Interaction

Another interesting property to investigate is the effective on-site density-density interaction, which is defined at $\lambda = 0$

$$U_{\text{eff}}(i\omega_n) \stackrel{\text{def}}{=} U + \mathcal{D}(i\omega_n)$$

and is frequency dependent. From Fig.9 we can see clearly that as the transition is approached, there is a tendency of the softening of the effective interaction at the zero frequency. In our model the frequency dependence of the local U_{eff} is due to screening of the bare interaction by the *intersite* Coulomb interaction V . Notice however that a frequency dependent U occurs more generally in realistic models of correlated electron due to *intrasite* screening by other local orbitals as a recent local GW calculation²¹ shows. This is the first E-DMFT study of a model where the interaction U is frequency dependent. We should stress that this behavior of the single particle Green's function can not be described by an ordinary DMFT with fixed U . In Fig.10 we show how the frequency depending effective U changes the single electron behavior. We plot in Fig.10 the imaginary part of the electron self-energy as a function of the Matsubara frequency. At high frequencies, the self-energy from E-DMFT coincides with that calculated using the bare U alone. This tells that the screening effect is not effective in the high frequency limit, same as we can see from the effective U plotted in Fig.9. In the low frequencies, the self-energy deviates to that of a smaller effective U . In Fig.10 we plotted the self-energies calculated at $V = 0$ and $U^{\text{eff}} = U_{\text{eff}}(i\omega_n)$ evaluated at the lowest and the next lowest Matsubara frequencies. We can see that at the first Matsubara frequency the E-DMFT self-energy is closest to that given by $U_{\text{eff}}(i\omega_1)$ and $V = 0$. We can understand the situation by thinking that there are two different U 's controlling low and high frequency regions separately. Some effective and screened U is in charge of the low frequency behavior while the bare U works in the high frequency region. In between there is a kind of the crossover connecting the two. The results shown here suggests that a frequency independent effective U is not enough to capture the physics in

the entire frequency range.

The set of diagrams presented above are plotted very close to the line of the Mott crossover (see Fig.1). In the following, we show two other sets of data which are plotted in the metallic and the Mott insulator phases, respectively.

C. Metallic Phase

First, we show the results at $U = 2.0$ and increasing V in Figs.11-13. As can be seen from Fig.1, at this set of parameters the system is in the correlated metallic phase. To be concise, we show here three representative plottings, that is the electron and phonon Green's functions and the electron self-energy. One can see that in this phase the change of the single electron Green's function is very limited as the transition is approached at $V \sim 0.95$. Meanwhile, the single electron self-energy changes quite a lot in the low frequency region, showing the stronger cancellation between the effects from U and V and thus the more significant reduction of the self-energy as V is increased. The change of the phonon Green's function is again much bigger than those of the electrons.

D. Paramagnetic Mott Insulating Phase

The second case with $U = 4.0$ is shown in Figs.14-16. Here we work in the Mott insulating phase. One can see from the asymptotic behavior of the Green's functions in the low frequency limit that in entire the range, especially near the transition at $V_c \sim 3.4$, the system is still in the Mott insulating phase. Meanwhile, the corresponding phonon Green's functions plotted in Fig.16 change a lot.

E. Phase Diagram

Finally, by literally sweeping across the U - V space, we are able to establish the finite temperature phase diagram presented in Fig.1. The phase transition from the metallic and the MI phases to the BI phase is determined unambiguously from the breaking down of the convergence of the E-DMFT iterations. We locate the crossover line between the FL and MI phases by search the points of (U,V) at which $\text{Im}G(ip_0) = -0.5$. While its specific value is arguable, this criterion works well practically in the sense that right around the CP it suggests, $(U_c, V_c) \sim (3.0, 1.6)$, we experienced the strongest critical slowing down.

Two remarks are in place concerning the qualitative features contained in this finite temperature phase diagram. First, the slopes of the boundaries of the FL phase are positive on both sides. This actually reflects the competition between U and V : The existence of a finite and small V requires a bigger U in order to make the Mott transition or crossover. Similarly a finite and small U makes it harder to develop the CDW. Second, the effects of a finite V is much stronger than that of U , because of the coordination number, which is six in the current case. The above features will retain in the phase diagram at $T = 0$.

V. E-DMFT PLUS C-DMFT FOR SYSTEMS WITH TWO SUBLATTICES

Next we consider E-DMFT on systems with two interpenetrating sublattices. The current study is useful in the situation when the two sublattices are not equivalent in the sense that, while it is homogeneous within each of them, the order parameter is different in the two sublattices. One then needs in E-DMFT a cluster containing at least two neighboring sites. It is interesting, though, to notice that the formalism we are going to develop also applies to the homogeneous systems. In this case the cluster plays the role to improve the description of the spatial correlations. The formalism described in this section can be easily

extended to problems where clusters of bigger sizes are needed. E-DMFT was combined with Dynamical Cluster Approximation (DCA) in Ref.[4].

Under the given conditions, the nearest neighbor hoppings and interactions always connect the two different sublattices, the next nearest neighbor ones are within the same sublattice, *etc.* We rely on the external magnetic fields introduced at the beginning, Eq.(1), to lift any possible degeneracy in the ground state. To illustrate the basic idea while avoid any unnecessary repetition (as it will turn out, the E-DMFT with two sublattices shares many properties with that for the homogeneous system), we work on a model with only nearest neighbor hoppings and density-density interactions, besides the on-site energy (the chemical potential) and the Hubbard interaction. The Hamiltonian reads:

$$\begin{aligned} \hat{H} = & -t \sum_{\langle Ai, Bj \rangle \sigma} (\hat{c}_{Ai, \sigma}^\dagger \hat{c}_{Bj, \sigma} + \text{h.c.}) - \sum_{Xi, \sigma} \mu_{Xi, \sigma} \hat{n}_{Xi, \sigma} \\ & + U \sum_{Xi} \hat{n}_{Xi, \uparrow} \hat{n}_{Xi, \downarrow} + \sum_{\langle Ai, Bj \rangle} (\hat{n}_{Ai, \uparrow} + \hat{n}_{Ai, \downarrow}) V_{Ai, Bj} (\hat{n}_{Bj, \uparrow} + \hat{n}_{Bj, \downarrow}), \end{aligned} \quad (32)$$

where every site is labeled by Xi with X labeling the two sublattices, $X = A, B$, and i the coordinate within the sublattice. $\langle Ai, Bj \rangle$ represents a pair of neighboring sites. We choose the chemical potential consistent with the two sublattice picture:

$$\mu_{Xi, \sigma} = \begin{cases} \mu_{A\sigma} & X = A \\ \mu_{B\sigma} & X = B \end{cases} \quad (33)$$

We set for nearest neighbors $V_{\langle Ai, Bj \rangle} = V \neq 0$. We then introduce the λ term same as before

$$\tilde{V}_{Xi, Yj} = \lambda \delta_{XY} \delta_{ij} - V_{Xi, Yj}$$

with λ a constant which ensures the $\tilde{V}_{2 \times 2}$ matrix to be positive-definite. After normal ordering the operators in the interactions and performing the Hubbard-Stratonovich transform, we have the effective action:

$$S = \int_0^\beta d\tau \left\{ \sum_{Xi, \sigma} [c_{Xi, \sigma}^\dagger(\tau) \partial_\tau c_{Xi, \sigma}(\tau) - \mu_{Xi, \sigma}^{\text{eff}} n_{Xi, \sigma}(\tau)] \right.$$

$$\begin{aligned}
& -t \sum_{\langle Ai, Bj \rangle, \sigma} [c_{Ai, \sigma}^\dagger(\tau) c_{Bj, \sigma}(\tau) + \text{h.c.}] + U^{\text{eff}} \sum_{Xi} : n_{Xi, \uparrow}(\tau) :: n_{Xi, \downarrow}(\tau) : \\
& + \frac{1}{2} \sum_{Xi, Yj} : \phi_{Xi}(\tau) : \tilde{V}_{Xi, Yj}^{-1} : \phi_{Yj}(\tau) : - \sum_{Xi} : \phi_{Xi}(\tau) :: [n_{Xi, \uparrow}(\tau) + n_{Xi, \downarrow}(\tau)] : \}, \quad (34)
\end{aligned}$$

with

$$\mu_{X, \sigma}^{\text{eff}} = \mu_{X, \sigma} - \frac{1}{2} U - \sum_j V_{\langle Xi, \bar{X}j \rangle} \langle [n_{\bar{X}j, \uparrow}(\tau) + n_{\bar{X}j, \downarrow}(\tau)] \rangle,$$

$$U^{\text{eff}} = U + \lambda,$$

where $\bar{X} = B$ if $X = A$ and vice versa. The Green's functions we are going to use are defined as follows:

$$G_\sigma^{\text{XY}}(i\tau|i'\tau') \stackrel{\text{def}}{=} -\langle \mathbf{T}_\tau c_{Xi, \sigma}(\tau) c_{Yi', \sigma}^\dagger(\tau') \rangle, \quad (35)$$

$$\chi^{\text{XY}}(i\tau|i'\tau') \stackrel{\text{def}}{=} -\langle \mathbf{T}_\tau : [n_{Xi, \uparrow}(\tau) + n_{Xi, \downarrow}(\tau)] :: [n_{Yi', \uparrow}(\tau') + n_{Yi', \downarrow}(\tau')] : \rangle, \quad (36)$$

$$D^{\text{XY}}(i\tau|i'\tau') \stackrel{\text{def}}{=} -\langle \mathbf{T}_\tau : \phi_{Xi}(\tau) :: \phi_{Yi'}(\tau') : \rangle. \quad (37)$$

The Dyson equations are now 2×2 matrix equations:

$$\begin{bmatrix} G_\sigma^{\text{AA}} & G_\sigma^{\text{AB}} \\ G_\sigma^{\text{BA}} & G_\sigma^{\text{BB}} \end{bmatrix}^{-1} (k, ip_n) = \begin{bmatrix} ip_n + \mu_{A\sigma} & -t_k \\ -t_{-k} & ip_n + \mu_{B\sigma} \end{bmatrix} - \begin{bmatrix} \Sigma_\sigma^{\text{AA}} & \Sigma_\sigma^{\text{AB}} \\ \Sigma_\sigma^{\text{BA}} & \Sigma_\sigma^{\text{BB}} \end{bmatrix} (k, ip_n). \quad (38)$$

$$\begin{bmatrix} D^{\text{AA}} & D^{\text{AB}} \\ D^{\text{BA}} & D^{\text{BB}} \end{bmatrix}^{-1} (k, i\omega_n) = - \begin{bmatrix} \lambda & -2V_k \\ -2V_{-k} & \lambda \end{bmatrix}^{-1} - \begin{bmatrix} \Pi^{\text{AA}} & \Pi^{\text{AB}} \\ \Pi^{\text{BA}} & \Pi^{\text{BB}} \end{bmatrix} (k, i\omega_n) \quad (39)$$

In the above equations and for all those with two sublattices, we always define the momentum in the reduced Brillouin zone. If the lattice under consideration is of supercubic type in d -dimension, one can easily find that for the nearest neighbor hopping and interaction, $t_k = t \sum_{i=1}^d \cos k_i$ and $V_k = V \sum_{i=1}^d \cos k_i$. Similar as that for the homogeneous system, we can derive an identity relating the phonon and the electron density Green's functions

$$\begin{bmatrix} \chi^{AA} & \chi^{AB} \\ \chi^{BA} & \chi^{BB} \end{bmatrix}^{-1}(k, i\omega_n) = \begin{bmatrix} \lambda & -2V_k \\ -2V_{-k} & \lambda \end{bmatrix} + \begin{bmatrix} \Pi^{AA} & \Pi^{AB} \\ \Pi^{BA} & \Pi^{BB} \end{bmatrix}^{-1}(k, i\omega_n). \quad (40)$$

We are now in the position to introduce the E-DMFT approximation. Following the same procedure as before, we can write down the effective E-DMFT action by using the cavity construction. What we do here is that we first integrate out all, including those in both sublattices, but two neighboring lattice sites, one from each of the two sublattices. In this way, we keep a cluster containing two representative lattice sites. The cluster plays the role as a composite impurity which is coupled to the self-consistent fermionic and bosonic baths. As we have mentioned earlier, it is found³³ that the Hartree terms from the non-local interaction across the cluster boundary contribute to the effective action. However, since the Hamiltonian we use here is prepared in such a way that there is no longer Hartree terms contained in the interaction, the procedure towards E-DMFT becomes very straightforward. The effective action is given by:

$$\begin{aligned} S^{\text{eff}} = & - \int_0^\beta d\tau \int_0^\beta d\tau' \sum_{XY,\sigma} c_{X,\sigma}^\dagger(\tau) [\mathcal{G}_\sigma^{XY}]^{-1}(\tau - \tau') c_{Y,\sigma}(\tau') \\ & - \frac{1}{2} \int_0^\beta d\tau \int_0^\beta d\tau' \sum_{XY} : \phi_X(\tau) : [\mathcal{D}^{XY}]^{-1}(\tau - \tau') : \phi_Y(\tau') : \\ & + U^{\text{eff}} \int_0^\beta d\tau \sum_X : n_{X,\uparrow}(\tau) :: n_{X,\downarrow}(\tau) : - \int_0^\beta d\tau \sum_X : \phi_X(\tau) :: [n_{X,\uparrow}(\tau) + n_{X,\downarrow}(\tau)] : \end{aligned} \quad (41)$$

with X, Y summed over A, B. From the effective action, we can measure the impurity Green's functions and calculate the self-energies by using the local Dyson equations. The self-consistency is reached by identifying the impurity Green's functions with the local Green's functions which are given as follows:

$$\begin{aligned} & \begin{bmatrix} G_\sigma^{\text{loc},AA} & G_\sigma^{\text{loc},AB} \\ G_\sigma^{\text{loc},BA} & G_\sigma^{\text{loc},BB} \end{bmatrix}(ip_n) = \sum_k \begin{bmatrix} G_\sigma^{AA} & G_\sigma^{AB} \\ G_\sigma^{BA} & G_\sigma^{BB} \end{bmatrix}(k, ip_n) \\ & = \sum_k \left\{ \begin{bmatrix} ip_n + \mu_{A\sigma} & t_k \\ t_{-k} & ip_n + \mu_{B\sigma} \end{bmatrix} - \begin{bmatrix} \Sigma_\sigma^{AA}(ip_n) & \Sigma_\sigma^{AB}(ip_n) \\ \Sigma_\sigma^{BA}(ip_n) & \Sigma_\sigma^{BB}(ip_n) \end{bmatrix} \right\}^{-1} \end{aligned} \quad (42)$$

$$\begin{aligned}
& \begin{bmatrix} D^{\text{loc,AA}} & D^{\text{loc,AB}} \\ D^{\text{loc,BA}} & D^{\text{loc,BB}} \end{bmatrix} (i\omega_n) = \sum_k \begin{bmatrix} D^{\text{AA}} & D^{\text{AB}} \\ D^{\text{BA}} & D^{\text{BB}} \end{bmatrix} (k, i\omega_n) \\
& = - \sum_k \left\{ \begin{bmatrix} \lambda & -2V_k \\ -2V_{-k} & \lambda \end{bmatrix}^{-1} + \begin{bmatrix} \Pi^{\text{AA}}(i\omega_n) & \Pi^{\text{AB}}(i\omega_n) \\ \Pi^{\text{BA}}(i\omega_n) & \Pi^{\text{BB}}(i\omega_n) \end{bmatrix}^{-1} \right\} \quad (43)
\end{aligned}$$

$$\begin{aligned}
& \begin{bmatrix} \chi^{\text{loc,AA}} & \chi^{\text{loc,AB}} \\ \chi^{\text{loc,BA}} & \chi^{\text{loc,BB}} \end{bmatrix} (i\omega_n) = \sum_k \begin{bmatrix} \chi^{\text{AA}} & \chi^{\text{AB}} \\ \chi^{\text{BA}} & \chi^{\text{BB}} \end{bmatrix} (k, i\omega_n) \\
& = \sum_k \left\{ \begin{bmatrix} \lambda & -2V_k \\ -2V_{-k} & \lambda \end{bmatrix} + \begin{bmatrix} \Pi^{\text{AA}}(i\omega_n) & \Pi^{\text{AB}}(i\omega_n) \\ \Pi^{\text{BA}}(i\omega_n) & \Pi^{\text{BB}}(i\omega_n) \end{bmatrix}^{-1} \right\}^{-1}. \quad (44)
\end{aligned}$$

Same as before, the λ dependences cancel out exactly. Combining the last two of the self-consistent equations, (43) and (44), we obtain the following identity:

$$\begin{aligned}
& \begin{bmatrix} \chi^{\text{loc,AA}}(i\omega_n) & \chi^{\text{loc,AB}}(i\omega_n) \\ \chi^{\text{loc,BA}}(i\omega_n) & \chi^{\text{loc,BB}}(i\omega_n) \end{bmatrix} = \begin{bmatrix} \Pi^{\text{AA}}(i\omega_n) & \Pi^{\text{AB}}(i\omega_n) \\ \Pi^{\text{BA}}(i\omega_n) & \Pi^{\text{BB}}(i\omega_n) \end{bmatrix} \times \\
& \left\{ \begin{bmatrix} 1 & 0 \\ 0 & 1 \end{bmatrix} + \begin{bmatrix} D^{\text{loc,AA}}(i\omega_n) & D^{\text{loc,AB}}(i\omega_n) \\ D^{\text{loc,BA}}(i\omega_n) & D^{\text{loc,BB}}(i\omega_n) \end{bmatrix} \begin{bmatrix} \Pi^{\text{AA}}(i\omega_n) & \Pi^{\text{AB}}(i\omega_n) \\ \Pi^{\text{BA}}(i\omega_n) & \Pi^{\text{BB}}(i\omega_n) \end{bmatrix} \right\} \quad (45)
\end{aligned}$$

It is not difficult to check that the above equation can be obtained directly from the effective action, Eq.(41). One needs only to write down the phonon Green's function and then integrate out the auxiliary fields. By using the local phonon Dyson equation, which is the matrix version of Eq.(16), one recovers Eq.(45).

This completes the formulation of E-DMFT with two sublattices. One can see that the theory easily combines E-DMFT with C-DMFT. We employ here a cluster of two sites, with the application in mind which will be discussed in §VII. There is, however, no difficulty to extend the formalism to clusters of any size.

VI. GW METHOD COMBINED WITH E-DMFT

As we have mentioned, C-DMFT⁶ allows to pick out a representative lattice cluster, instead of a single site, in order to describe a many body system. This makes possible to treat the finite range interaction as well as the broken symmetry phase *within* the cluster. The advantage of C-DMFT is that it solves exactly the cluster so that the spatially non-local correlations within the cluster are automatically taken into account. In combining with E-DMFT, C-DMFT is also able to handle interactions with range beyond the cluster size, as we have shown in the last section. However, the price one has to pay is that in solving a cluster, a lot more technical resources are needed.

In this section we propose a less computationally intensive prescription as compared to the E-DMFT + C-DMFT procedure. It is based on the following physical idea. In real materials, the on-site Hubbard interaction U is much larger than the non-local ones. Hence the local interaction has to be treated non-perturbatively (namely with DMFT) in order to obtain the local self-energy. Meanwhile it is legitimate to make perturbative expansion to obtain the non-local part of the self-energy in the spirit of the GW method²⁴. The original GW method computes a screened Coulomb line W by summing Random Phase Approximation (RPA) diagrams and obtains the one electron self-energy by considering the lowest order graph in W , hence the name GW. The E-DMFT-GW approach is derivable via the Baym-Kadanoff functional¹⁷. The functional derivatives of the 2-particle irreducible part of the Baym-Kadanoff functional, $\Phi(G, D)$, with respect to the full Green's function give the corresponding self-energies. $\Phi(G, D)$ is constructed with the full Green's functions G and D and the interaction vertices (As discussed in §VIII, the choice of the phonon field should be done judiciously). The E-DMFT-GW method consists of approximating Φ (see Fig.17) by the leading order non-local graphs and evaluating the rest of the functional Φ in the local approximation. The E-DMFT-GW self-energies are given by

$$\begin{aligned}\Sigma_{\sigma;i,j}(G, D) &= \frac{\delta\Phi(G, D)}{\delta G_{\sigma;i,j}} \simeq \delta_{ij}\Sigma_{\sigma;i,i}^{\text{E-DMFT}}(G, D) + (1 - \delta_{ij})\Sigma_{\sigma;i,j}^{\text{GW}}(G, D) \\ \Pi_{i,j}(G, D) &= \frac{\delta\Phi(G, D)}{\delta D_{i,j}} \simeq \delta_{ij}\Pi_{i,i}^{\text{E-DMFT}}(G, D) + (1 - \delta_{ij})\Pi_{i,j}^{\text{GW}}(G, D)\end{aligned}\quad (46)$$

For the approach to be derivable from a functional, $\Sigma(G, D)$ and $\Pi(G, D)$ has to be calculated self-consistently. The GW method has been applied in *ab initio* calculations of semiconductors since the original works by G. Strinati, H.J. Mattausch, and W. Hanke⁴⁰. However, it was pointed out that in LDA-GW for electron systems⁴¹ the self-consistency results in incorrect one-electron spectra and that it is better to compute $\Sigma(G_0)$ with G_0 the unperturbed Green's function instead. Better total energy, though, is obtained from $\Sigma(G)$ ^{41,42}. We believe that our proposal resolves this contradiction. The E-DMFT iteration obtains the largest self-energy term (the on-site one) self-consistently and non-perturbatively. The GW approximation is used for the smaller term (the off-diagonal one). In our model calculation we find the difference between E-DMFT + non-self-consistent GW and E-DMFT + self-consistent GW is small. This can be generalized in a straightforward way to realistic multiband situations.

We need to discuss more specifically the non-local self-energy diagrams in our generalized GW approach in combination with the E-DMFT. We identify two such contributions. The first is the boson exchange diagram which is of the same form as that in the GW method [Fig.18(B1)]. We require that the two vertices Γ_3 be local and come from different lattice sites, giving rise to the off-diagonal self-energy. Fig.18(B1) uses the full electron-phonon vertices, instead of the bare ones, in the exchange diagram of the self-energy. Those local vertices, which can be measured in E-DMFT-QMC, are defined through the following Green's function⁴³:

$$\begin{aligned}G^{\text{loc}}(\tau_1\sigma_1, \tau_2\sigma_2; \tau_3) &\stackrel{\text{def}}{=} \langle \mathbf{T}_{\tau} c_{\sigma_1}(\tau_1) c_{\sigma_2}^{\dagger}(\tau_2) \phi(\tau_3) \rangle \\ &= \int_0^{\beta} d\tau'_1 \sum_{\sigma'_1} \int_0^{\beta} d\tau'_2 \sum_{\sigma'_2} \int_0^{\beta} d\tau'_3 G^{\text{loc}}(\tau_1\sigma_1|\tau'_1\sigma'_1) G^{\text{loc}}(\tau_2\sigma_2|\tau'_2\sigma'_2)\end{aligned}$$

$$\Gamma_3^{\text{loc}}(\tau'_1\sigma'_1, \tau'_2\sigma'_2; \tau'_3)D^{\text{loc}}(\tau'_3|\tau_3). \quad (47)$$

Unlike the skeleton diagram commonly used for the electron self-energy⁴³ where one of the vertices should be bare to avoid over-counting, the diagram Fig.18(B1) uses two full local vertices. Our requirement, that the two vertices be from different lattice sites, ensures that there is no over-counting. While the skeleton construction uses one bare and one full vertex to produce the exact self-energy, our method uses two full local vertices to produce the leading non-local correction. We should also remark that both the electron and phonon lines appeared in Fig.18(B1) represent the non-perturbative Green's functions from E-DMFT. Especially, the phonon Green's function plays the role as the screened Coulomb interaction which in the original GW is obtained by using RPA.

There is another contribution, which originates from the local interaction U at the second order [Fig.18(B2)]. The reason this contribution is important is that usually U is much bigger than V . The effective local vertex Γ_4^{loc} is defined in the following way:

$$\begin{aligned} G^{(2),\text{loc}}(\tau_1\sigma_1, \tau_2\sigma_2|\tau_3\sigma_3, \tau_4\sigma_4) &\stackrel{\text{def}}{=} \langle T_\tau c_{\sigma_1}(\tau_1)c_{\sigma_2}(\tau_2)c_{\sigma_3}^\dagger(\tau_3)c_{\sigma_4}^\dagger(\tau_4) \rangle \\ &= G^{\text{loc}}(\tau_1\sigma_1|\tau_4\sigma_4)G^{\text{loc}}(\tau_2\sigma_2|\tau_3\sigma_3) - G^{\text{loc}}(\tau_2\sigma_2|\tau_4\sigma_4)G^{\text{loc}}(\tau_1\sigma_1|\tau_3\sigma_3) \\ &+ \int_0^\beta d\tau'_1 \sum_{\sigma'_1} \int_0^\beta d\tau'_2 \sum_{\sigma'_2} \int_0^\beta d\tau'_3 \sum_{\sigma'_3} \int_0^\beta d\tau'_4 \sum_{\sigma'_4} G^{\text{loc}}(\tau_1\sigma_1|\tau'_1\sigma'_1)G^{\text{loc}}(\tau_2\sigma_2|\tau'_2\sigma'_2) \\ &\quad \Gamma_4^{\text{loc}}(\tau'_1\sigma'_1, \tau'_2\sigma'_2|\tau'_3\sigma'_3, \tau'_4\sigma'_4)G^{\text{loc}}(\tau'_3\sigma'_3|\tau_3\sigma_3)G^{\text{loc}}(\tau'_4\sigma'_4|\tau_4\sigma_4) \end{aligned} \quad (48)$$

If there is no external magnetic field, only two spin configurations are allowed in the two particle Green's function as well as the vertex, that with all the spins in the same direction and that with two spins up and two spins down⁴⁴. Once we get the local vertex, the corresponding contribution to the off-site self-energy can be constructed as shown in Fig.18(B2), with again the vertices coming from different sites and ensuring no double counting of the

diagrams. It should also be pointed out that the diagrams contained in Fig.18(B1) and (B2) are totally different. This can be seen easily by comparing the non-local lines in the two diagrams.

To compare the importance of the two terms, we can investigate their scaling behavior with the spatial dimension⁴⁵. We should keep in mind that both G and W scale as $1/\sqrt{d}$ for nearest neighbors in real space, with d the dimension, and both the interaction vertices are local which means they do not scale. We then see that the leading electron-phonon contribution scales as $1/d$ and that of the on-site interaction as $1/d^{3/2}$. In the infinite dimension limit there is no doubt that the electron-phonon contribution is more important. However, if we work in finite spatial dimensions (usually ≤ 3) and since the on-site interaction U is likely much bigger than the off-site one, V , these two can be of the same order practically. This actually happens in the example in 1-D which we will show in the next section.

In the same spirit one can also obtain the leading non-local correction to the phonon self-energy, *i.e.* Fig.18B(3), which is the leading non-local correction in terms of the E-DMFT interactions. Due to the two electron lines, the diagram scales as $1/d$ when the two contributing lattice sites are nearest neighbors.

In practical calculations, we first solve E-DMFT iteratively and obtain all the local self-energies and the interaction vertices. We then apply GW approximation to calculate the non-local self-energies by using the Green's functions obtained from E-DMFT. As in the original GW, we assume here that the corrections do not change dramatically the physical properties of the system so that we are allowed to use the quantities from E-DMFT directly. The last step is to use the approximate self-energies in the exact Dyson equation so that all the Green's functions, with both spatial and temporal dependences, can be calculated.

The GW contributions to the self-energies are calculated in the real space-time as follows

for $i \neq j$ (see Fig.18)

$$\begin{aligned}
\Sigma_{\sigma}^{\text{GW}}(i\tau|j\tau') &= - \int_0^{\beta} d\tau_1 \sum_{\sigma_1} \int_0^{\beta} d\tau_1' \sum_{\sigma_1'} \int_0^{\beta} d\tau_2 \int_0^{\beta} d\tau_2' \\
&\Gamma_{3,i}^{\text{loc}}(\tau\sigma, \tau_1\sigma_1; \tau_2) G(i\tau_1\sigma_1|j\tau_1'\sigma_1') D(i\tau_2|j\tau_2') \Gamma_{3,j}^{\text{loc}}(\tau_1'\sigma_1', \tau'\sigma; \tau_2) \\
&- \int_0^{\beta} d\tau_1 \sum_{\sigma_1} \int_0^{\beta} d\tau_1' \sum_{\sigma_1'} \int_0^{\beta} d\tau_2 \sum_{\sigma_2} \int_0^{\beta} d\tau_2' \sum_{\sigma_2'} \int_0^{\beta} d\tau_3 \sum_{\sigma_3} \int_0^{\beta} d\tau_3' \sum_{\sigma_3'} \\
&\Gamma_{4,i}^{\text{loc}}(\tau\sigma, \tau_1\sigma_1|\tau_2\sigma_2, \tau_3\sigma_3) G(i\tau_1\sigma_1|j\tau_1'\sigma_1') G(i\tau_2\sigma_2|j\tau_2'\sigma_2') G(j\tau_3'\sigma_3'|i\tau_3\sigma_3) \Gamma_{4,j}^{\text{loc}}(\tau_3'\sigma_3', \tau_2'\sigma_2'|\tau_1'\sigma_1', \tau'\sigma)
\end{aligned} \tag{49}$$

$$\begin{aligned}
\Pi^{\text{GW}}(i\tau|j\tau') &= \int_0^{\beta} d\tau_1 \sum_{\sigma_1} \int_0^{\beta} d\tau_1' \sum_{\sigma_1'} \int_0^{\beta} d\tau_2 \sum_{\sigma_2} \int_0^{\beta} d\tau_2' \sum_{\sigma_2'} \\
&\Gamma_{3,i}^{\text{loc}}(\tau_1\sigma_1, \tau_2\sigma_2; \tau) G(i\tau_1\sigma_1|j\tau_1'\sigma_1') G(j\tau_2'\sigma_2'|i\tau_2\sigma_2) \Gamma_{3,j}^{\text{loc}}(\tau_2'\sigma_2', \tau_1'\sigma_1'; \tau')
\end{aligned} \tag{50}$$

In the above equations we labeled the vertices by the lattice site index with in mind the possibility of inequivalent sublattices. There is a symmetry one can use in the calculation at $i \neq j$:

$$G_{\sigma}(i\tau|j\tau') = [G_{\sigma}(j\tau'|i\tau)]^{\dagger} \tag{51}$$

It is both physically transparent and technically convenient to perform the generalized GW calculation in the coordinate space and imaginary time⁴⁶. It is also very easy to extend the expressions to the systems with different sublattices, as we will show in the next section.

VII. APPLICATION II: 1D BAND INSULATOR VIA E-DMFT PLUS GW

Since we want to investigate if the GW method can improve the E-DMFT results, we need to know the corresponding exact solution of the model under investigation. In this

section, we implement the E-DMFT of two sublattices for a 1D U-V model with an alternating chemical potential. This model can be solved exactly at $T = 0$ via Density Matrix Renormalization Group (DMRG)^{47,48}. The model is relevant in the study of the interplay between the electronic correlation and the electron-phonon coupling in the mixed stack organic compounds^{29,30} and the ferroelectric perovskites³¹. The phase diagram has been studied⁴⁹.

Because we solve the impurity model in E-DMFT using QMC simulation which works at finite temperatures, we need to make the comparison in the band insulating phase where all the excitations are gapped so that the effects of the thermal excitations are suppressed at low enough temperatures. We also want to make the comparison in the parameter space where the quantum fluctuation is strong enough so that the standard mean field solution does not work. It is known that in such a case one needs C-DMFT of at least two sites to get good agreement with the exact solution³³. Our goal here, though, is mainly to see if the GW method can improve the E-DMFT results.

Due to the above reasons, the E-DMFT we are going to use in this section is slightly different from that described in §V which combined E-DMFT with C-DMFT. The *pure* E-DMFT (without C-DMFT) for two sublattices is established in the following way. We first choose a representative site from sublattice A, integrate out all the other sites in both the sublattices, and obtain an effective impurity action for this site. Then, from the nearest neighbors of this site, we choose another representative site, which obviously belongs to sublattice B, and repeat the same procedure. The two effective actions reached in this way are the same as that for a homogeneous system we described in §III. They are formally independent to each other at the level of the impurity model. Of course the two are connected, at the self-consistency, through the Dyson equations which are the same as those given by Eqs. (38) and (39), except the off-diagonal self-energies are now zero. Technically, one can easily understand the structure of this E-DMFT by imposing the requirement on all the corresponding equations in §V that the impurity model be restrictively local. Then all the

off-diagonal dynamical Weiss fields, and thus the off-diagonal self-energies, are zero. However, the impurity Green's functions still have non-local contributions, as is evident from Eqs.(42)-(44). This scenario of implementing (E-) DMFT, in midway between the single site (E-) DMFT and the cluster one, has been used successfully in treating systems with inequivalent sublattices while avoiding the heavy calculations needed in C-DMFT¹.

We study here the following Hamiltonian:

$$\begin{aligned} \hat{H} = & -t \sum_{i,\sigma} (\hat{c}_{i,\sigma}^\dagger \hat{c}_{i+1,\sigma} + \text{h.c.}) - \sum_{i,\sigma} \mu_i \hat{n}_{i,\sigma} \\ & + U \sum_i (\hat{n}_{i,\uparrow} - \frac{1}{2})(\hat{n}_{i,\downarrow} - \frac{1}{2}) + V \sum_i (\hat{n}_{i,\uparrow} + \hat{n}_{i,\downarrow} - 1)(\hat{n}_{i+1,\uparrow} + \hat{n}_{i+1,\downarrow} - 1). \end{aligned} \quad (52)$$

We consider the special case with alternating chemical potential:

$$\mu_i = (-1)^i \mu \quad (53)$$

In this case we know the exact forms of the hopping matrix element and the non-local interaction. We can write down for the off-diagonal terms in the Dyson equations (38) and (39)

$$t_k = t e^{ik} \cos k, \quad V_k = V e^{ik} \cos k \quad (54)$$

The momentum k is again restricted in the reduced Brillouin zone, given by $-\pi/2 < k \leq \pi/2$ in the current case. The phase factors $\exp(\pm ik)$ come from the fact that each site (A,i) [(B,i)] has two neighbors, one within the same unit cell, (B,i) [(A,i)] and the other comes from the cell to the left (right), (B,i-1) [(A,i+1)]. Hence the later contributes a momentum dependent phase factor. Remember when we use the above two equations for self-consistency in E-DMFT, the off-diagonal self-energies for both electrons and phonons should be set to zero due the assumption of locality:

$$\Sigma_\sigma^{\text{AB}}(ip_n) = 0, \quad \Pi^{\text{AB}}(i\omega_n) = 0. \quad (55)$$

Because of the dimensionality, the momentum summations needed in calculating the local Green's functions can be carried out exactly, which give:

$$G_{\sigma}^{\text{loc,XX}}(ip_n) = \sum_k G_{\sigma}^{\text{XX}}(k, ip_n) = \frac{\zeta_{\sigma}^{\overline{\text{XX}}}(ip_n)}{\zeta_{\sigma}^{\text{AA}}(ip_n)\zeta_{\sigma}^{\text{BB}}(ip_n) - 1} \quad (56)$$

with

$$\zeta_{\sigma}^{\text{X}}(ip_n) \stackrel{\text{def}}{=} ip_n + \mu_{\text{X}}^{\text{eff}} - \Sigma_{\sigma}^{\text{XX}}(ip_n).$$

and

$$\begin{aligned} D^{\text{loc,XX}}(i\omega_n) &= \sum_k D^{\text{XX}}(k, i\omega_n) \\ &= \frac{4V^2\Pi^{\overline{\text{XX}}}}{\sqrt{1 - 4V^2\Pi^{\text{AA}}(i\omega_n)\Pi^{\text{BB}}(i\omega_n)}[1 + \sqrt{1 - 4V^2\Pi^{\text{AA}}(i\omega_n)\Pi^{\text{BB}}(i\omega_n)}]} \end{aligned} \quad (57)$$

In the above, we used again the notation that $\overline{\text{X}} = \text{B}$ if $\text{X} = \text{A}$ and vice versa. As we have noted, the solution of the impurity model in the current case consists of two independent parts, one for each representative lattice site, and each of them are exactly the same as that for a homogeneous system. The only difference comes in at the self-consistent conditions which are given by the above pair of equations.

After we get the solution of the impurity model, either within a single iteration or after the convergence of the E-DMFT iterations, we can perform the GW perturbative calculations. To illustrate the idea and see qualitatively how the GW self-energy can improve the results, we consider here the simplest and the most important GW contributions, those from the nearest neighbors. They contribute directly to the off-diagonal self-energies, while for the diagonal ones, we use those from the E-DMFT calculation. All the other contributions are neglected because the Green's functions decay exponentially as the spatial separation increases in the band insulating phase.

We can now write down the expression for the self-energy matrices as follows:

$$\begin{bmatrix} \Sigma_{\sigma}^{\text{AA}} & \Sigma_{\sigma}^{\text{AB}} \\ \Sigma_{\sigma}^{\text{BA}} & \Sigma_{\sigma}^{\text{BB}} \end{bmatrix} (k, ip_n) \simeq \begin{bmatrix} \Sigma_{\sigma}^{\text{DMFT,AA}}(ip_n) & \Sigma_{\sigma}^{\text{GW,AB}}(ip_n)e^{ik} \cos k \\ \Sigma_{\sigma}^{\text{GW,BA}}(ip_n)e^{-ik} \cos k & \Sigma_{\sigma}^{\text{DMFT,BB}}(ip_n) \end{bmatrix} \quad (58)$$

$$\begin{bmatrix} \Pi^{\text{AA}} & \Pi^{\text{AB}} \\ \Pi^{\text{BA}} & \Pi^{\text{BB}} \end{bmatrix} (k, i\omega_n) \simeq \begin{bmatrix} \Pi^{\text{DMFT,AA}}(i\omega_n) & \Pi^{\text{GW,AB}}(i\omega_n)e^{ik} \cos k \\ \Pi^{\text{GW,BA}}(i\omega_n)e^{-ik} \cos k & \Pi^{\text{DMFT,BB}}(i\omega_n) \end{bmatrix} \quad (59)$$

The momentum dependences of the off-diagonal terms in the above two equations come in for the same reason as those in the free electron and phonon propagators. In the current situation both the GW terms we discussed in the previous section contribute as given by Eqs.(49) and (50). To make life easier, we make a further approximation which replaces the full interaction vertices by their bare values:

$$\Gamma_3^{\text{loc}}(\tau_1\sigma_1, \tau_2\sigma_2; \tau_3) = \delta_{\sigma_1, \sigma_2} \delta(\tau_1 - \tau_2) \delta(\tau_1 - \tau_3), \quad (60)$$

$$\Gamma_4^{\text{loc}}(\tau_1\sigma_1, \tau_2\sigma_2 | \tau_3\sigma_3, \tau_4\sigma_4) = U \delta_{\sigma_1, \sigma_4} \delta_{\sigma_2, \sigma_3} \delta(\tau_1 - \tau_2) \delta(\tau_1 - \tau_3) \delta(\tau_1 - \tau_4). \quad (61)$$

Then Eqs.(49) and (50) are greatly simplified and give:

$$\Sigma_{\sigma}^{\text{GW}}(i\tau | j\tau') = -G_{\sigma}(i\tau | j\tau') D(i\tau | j\tau') - U^2 G_{-\sigma}(i\tau | j\tau') G_{-\sigma}(j\tau' | i\tau) G_{\sigma}(i\tau | j\tau'), \quad (62)$$

$$\Pi^{\text{GW}} = \sum_{\sigma} G_{\sigma}(i\tau | j\tau') G_{\sigma}(j\tau' | i\tau). \quad (63)$$

In reaching the numerical results we are going to present, we use $\lambda = 2.0$ for the positive-definiteness of the effective interaction matrix. In every iteration, the impurity model is solved via QMC by 10^6 sweeps. To reach the E-DMFT convergence, ten iterations are usually needed.

We first show in Fig.19 the temperature dependence of the imaginary part of the electron Green's function calculated at $U = 5.0$, $V = 0.5$, and $\mu = 2.0$. The three cases are calculated at three different inverse temperatures, $\beta = 5.0, 8.0, 10.0$, with the corresponding $\Delta\tau = 0.25, 0.20, 0.25$, respectively. It is obvious that the three sets of the data lie on a

single smooth curve. Actually this same situation happens for all the other quantities we measured which are not shown here. All these suggest that, at the given temperatures, with the highest at $T = 1/5.0$, the thermal fluctuations are already suppressed due the band gap and we need not worry about the temperature effects. In the following, we present the results calculated at $\beta = 5.0$.

In Fig.20 we present the data of the imaginary part of the electron Green's functions calculated using E-DMFT alone, using GW with the electron-phonon vertex [corresponding to Fig.18B(1)], and with the local Hubbard vertex [corresponding to Fig.18B(2)], respectively. In the latter two the GW calculations are performed after E-DMFT convergence. The exact result and the Hartree mean field (MF) result are also plotted as references. From the results, one can see that the two terms in the GW correction are of the same order.

In Fig.21 we show the results of the imaginary part of the local electron Green's function from GW calculation after E-DMFT convergence and those using GW within the E-DMFT iteration loop. One can see that the difference is very small. The corresponding real part is plotted in Fig.22. In Fig.23 we show the plotting of the Green's function between a pair of neighboring sites. We can also compare the result on the average energy per site ϵ . The result of GW after E-DMFT gives $\epsilon = -1.76$ and that for GW within E-DMFT $\epsilon = -1.74$. The DMRG finds the exact average ground state energy per site to be $\epsilon = -2.09$. The difference between the two GW+DMFT procedures is again very minor. From the given results and those performed at the other parameter points which are not shown here, we conclude that the two procedures, one with GW after E-DMFT and the other with GW in E-DMFT iteration, give very close results, although it seems the former is a little better.

The physical information contained in Figs.20-23 can be understood as follows. (i) In one dimension, all the allowed modes of the low energy excitations are those bosonic particle hole pairs carrying momentum $k \sim 0$ and $k \sim 2k_F$ ($= \pi$ at half-filling) with respect to the

Hartree ground state. This explains why a C-DMFT calculation with a cluster of only two sites gives quite good results³³ while the E-DMFT we employed here does not work very well at low frequencies. The difference is basically that a model of a single site can only capture those modes $k \sim 0$; but a cluster of two sites is already good enough for those at $k \sim \pi$.

(ii) Since the classical Hartree energy gap, which is given by $-U/2 + 2V + \mu = 0.5$ is quite small in this case and both the interactions in Eq.(52) are (marginally) relevant with respect to the metallic Gaussian fixed point, as we go to lower energy scales and thus longer wave lengths, the energy gap gets renormalized significantly. This explains why the exact DMRG result is so different from the MF result at low frequencies. The high frequency behavior, on the other hand, can be captured fairly well even by the Hartree approximation, which is evident from Figs.20-23. This is the region where all the different approaches converge to give the same result. (iii) From the figures of the local electron Green's function one can see that at not too low frequencies (basically, those beyond the first two Matsubara frequencies), the E-DMFT result is much better than the MF result and closer to the exact ones. This is consistent with the scaling picture since the contributions to the results at those frequencies higher than the gap energy, which is of the order of "1" in the current case, can only be from the local behavior and are described fairly well by the E-DMFT. On the other hand, this same reason explains the big deviation of the E-DMFT result at the first two Matsubara frequencies: They are affected more strongly by those quantum/thermal fluctuations with longer wave length, which are mostly neglected by the E-DMFT approximation. (iv) The GW works in the way we have anticipated. It incorporates more spatial correlations into the self-energy so that the low frequency behavior benefits a lot from the correction. As we can see from Figs.21 and 22 the GW contributes to both the real and imaginary parts of the local Green's functions corrections of more than 15%. (v) The GW method used here has little effect on the nearest neighbor Green's functions because it is designed to improve the local Green's functions.

What we have shown above is that the GW method can be used to improve the E-

DMFT results. Due to the dimensionality, the single-site E-DMFT results deviates from the exact ones at the lowest frequencies. By incorporating the spatial correlations, the GW perturbation contributes a desired correction. Of course in this very case in 1D it is known that the spatial correlation is so important that a leading order perturbation is not enough to recover the exact results. What is important is that the above example shows the GW method works in the way as we anticipated. Our major objective is to apply GW-DMFT to strongly correlated electronic systems in higher dimensions. we know E-DMFT works much better as is evident from the scaling behavior with respect to the dimension. We also know that the leading order perturbation in terms of the interaction vertex, the GW, works better. We thus have a method which is much easier to handle technically than C-DMFT and is able to achieve the same goal to certain extent.

VIII. FURTHER DEVELOPMENT AND OUTLOOK

E-DMFT allows to describe the interactions in a more flexible way than we have presented so far. The need for such a freedom is evident in the realistic calculation of materials, where, instead of the nearest neighbor repulsion considered in this paper we have to treat the Coulomb interaction and its multipole expansion. For such a system, the dielectric function is given by, in the linear response theory²²:

$$\epsilon^{-1}(q, i\omega_n) = 1 + v_q \chi(q, i\omega_n) \quad (64)$$

where v_q is the Coulomb interaction given by, in 3D

$$v_q = \frac{4\pi e^2}{q^2} \quad (65)$$

and $\chi(q, i\omega_n)$ is the density-density Green's function defined through Eq.(8). One can make use of the electron-phonon identity, Eq.(10) (set $\lambda = 0$) and get:

$$\epsilon(q, i\omega_n) = 1 - v_q \Pi(q, i\omega_n) \quad (66)$$

Here the phonon self-energy Π can be understood as the collection of all the electron polarization diagrams. If one proceeds with the formalism we presented in the previous sections, the phonon self-energy Π within E-DMFT approximation is assumed to be momentum independent. However, Eq.(66) is not the correct functional form for an insulator in which the polarization should be given by $\Pi(q, i\omega_n) \sim q^2 f(q, \omega_n)$ with f weakly q dependent.

To handle this situation in E-DMFT we have to tailor the formalism to be compatible with the functional form of the response function. This leads us to the following generalization of the action discussed in Sections II and III:

$$S = S_0 + \int_0^\beta d\tau \sum_q \left[\frac{1}{2} \sum_{a,b} \phi_a(q, \tau) D_{0,ab}^{-1}(q) \phi_b(-q, \tau) - \sum_{a;\alpha,\beta} \phi_a(q, \tau) \rho_a(-q) \right] \quad (67)$$

where we have defined a generalized electron density:

$$\rho_a(q) = \sum_k \sum_{\alpha\beta} c_{k+q/2,\alpha}^\dagger \Lambda_{a;\alpha\beta}(k+q/2, k-q/2) c_{k-q/2,\beta} \quad (68)$$

with α and β the spin labels. The indices a and b are used to label the local degrees of freedom other than the spin, like the components of the multipole moments. S_0 is the free action plus the local interaction. The key part here is the electron-phonon vertex $\Lambda_{a;\alpha,\beta}(k+q/2, k-q/2)$ which is momentum dependent. A wise choice of this vertex allows to preserve the physical momentum dependence in the response function after the E-DMFT approximation.

We can define the following Green's function in the matrix form:

$$\begin{aligned} [D(q, \tau)]_{ab} &= -\langle T_\tau \phi_a(q, \tau) \phi_b(-q, 0) \rangle \\ [\tilde{\chi}(q, \tau)]_{ab} &= -\langle T_\tau \rho_a(q, \tau) \rho_b(-q, 0) \rangle \\ &= \sum_{k,k'} \Lambda_{a,\alpha\beta}(k+q/2, k-q/2) \Lambda_{b,\alpha'\beta'}(k'-q/2, k'+q/2) \chi_{\alpha\beta,\alpha'\beta'}(k, q, \tau; k', -q, 0) \end{aligned} \quad (69)$$

with

$$\chi_{\alpha\beta,\alpha'\beta'}(k, q, \tau; k', q', 0) = -\langle T_\tau c_{k+q/2,\alpha}^\dagger(\tau) c_{k-q/2,\beta}(\tau) c_{k'+q'/2,\alpha'}^\dagger(0) c_{k'-q'/2,\beta'}(0) \rangle$$

Same as before, we can derive an electron-phonon identity:

$$[\tilde{\chi}(q, i\omega_n)]^{-1} = -D_0(q) + \Pi^{-1}(q, i\omega_n), \quad (70)$$

So far the results are exact. The E-DMFT approximation amounts to mapping the general model (67) to an impurity problem by integrating out all but one lattices site (we consider the homogeneous phase here). The only new feature is that the general electron-phonon interaction vertex is not necessarily local as we had before. The resulting phonon self-energy is a function of frequency only. However, the general density-density Green's function χ , a physical quantity, now contains a non-trivial momentum dependence which is evident from Eqs.(69) and (70). Since the electron-phonon vertex Λ can always be adjusted by redefining the auxiliary phonons, we are able to obtain the desired momentum dependence from the physical considerations.

To see how it works, we go back to the example of the insulator. We need the following form of the electron-phonon coupling in order to describe the dipole-dipole interaction:

$$\Lambda_{a,\alpha\beta}(k + q/2, k - q/2) = \delta_{\alpha\beta} \frac{q_a}{q^2} \quad (71)$$

with $a = x, y, z$. Meanwhile the free phonon propagator is of the form

$$D_{0,ab}(q) = \frac{\delta_{ab}}{4\pi e^2}, \quad (72)$$

in order that the Coulomb interaction be recovered when the auxiliary phonons are integrated out. Under this interaction vertex, the auxiliary phonon represents an electric field mediating the dipole-dipole interaction. Since only the longitudinal field is coupled to the dipole moment, we can keep the corresponding phonon mode and discard the transversal ones. For the E-DMFT approximation, it is desired to work in the coordinate space where the cavity construction is possible. To this end one needs to convert the electron-phonon

coupling to real space which can be done by using the Wannier functions.

After solving the E-DMFT problem, the electron density Green's function is given by

$$\chi(q, i\omega_n) = q^2 \frac{-\Pi(i\omega_n)}{1 + 4\pi e^2 \Pi(i\omega_n)} \quad (73)$$

and the dielectric function becomes

$$\epsilon(q, i\omega_n) = 1 + 4\pi e^2 \Pi(i\omega_n), \quad (74)$$

which has the correct form for an insulator.

To conclude, we have introduced in this section a way to tailor the E-DMFT formalism so that the desired momentum dependence can be preserved from physical considerations.

IX. CONCLUSION

In the paper we suggested a simple procedure of deriving E-DMFT formalism, that is first separating out the Hartree contributions and then making the E-DMFT approximation with regard to the fluctuations around the Hartree ground state. This procedure is essential in the phase with broken symmetry. It also helps to formulate the C-DMFT.

We developed an E-DMFT formulation by using a real Hubbard-Stratonovich transformation. We introduced a local shift to the general non-local interaction to ensure the positive-definiteness of the effective interaction matrix. Our investigation showed that in all the physical quantities the effects from the arbitrary shift canceled out exactly. We also proved the equivalence of forming the E-DMFT self-consistency by using the auxiliary phonon Green's function and the two-electron Green's function. Based on these ideas, we derived an E-DMFT of a single impurity site for a homogeneous system with generic two

particle interactions. We also presented a formalism of E-DMFT combined with C-DMFT for a cluster of two lattice sites, which is generalizable to clusters containing any number of sites.

We suggested a generalized GW approach to incorporate the spatial correlations into the E-DMFT approximation. While the on-site self-energies are obtained non-perturbatively through E-DMFT, those relatively weaker off-site contributions can be calculated in a perturbative way. We identified the most important contributions to the non-local self-energies.

We showed how E-DMFT could be tailored to handle the response functions with non-trivial momentum dependence in an insulator. Through the example of the dielectric function we exhibited that an appropriately defined electron-phonon vertex was able to keep the correct functional form of the response function.

We implemented a QMC algorithm with shifts in E-DMFT to handle the non-positive-definite interactions. This algorithm can be used for a large variety of problems, including the Anderson lattice with antiferromagnetic interactions. Two examples of the implementations were presented.

The first example was the application of the single site E-DMFT to the 3D U-V model. We studied the behavior of the electron Green's function and the response function as the density instability was approached. We studied the crossover between the metallic and the Mott insulating phases. We investigated the frequency dependence of the effective on-site interaction and showed its impact on the single electron behavior. We showed a finite temperature phase diagram of the 3D U-V model.

In the second example, we applied a single site E-DMFT combined with GW method to a 1D U-V model with an alternating chemical potential. It was found that the GW

approach improved the E-DMFT results at low frequencies in the desired direction. We also found that in the case under investigation, it made little difference whether or not the GW perturbation was performed within the E-DMFT iteration.

The success of the E-DMFT implementation opens the door to tackle many complicated physical problems which could not be handled by simple DMFT or other methods. The combination with GW and/or C-DMFT points out a systematic way to improve the (E-) DMFT method.

ACKNOWLEDGMENTS

This research was supported by NSF under Grant No. DMR-0096462 and by the Center for Materials Theory at Rutgers University. We would like to thank A. Georges, S. Florens, S. Savrasov, and V. Udovenko for useful discussions and C.J. Bolech and S.S. Kancharla for the use of their DMRG program.

REFERENCES

- ¹ A. Georges, G. Kotliar, W. Krauth, and M.J. Rozenberg, *Rev. Mod. Phys.* **68**, 13 (1996).
- ² P.G.J. van Dongen, *Phys. Rev. Lett.* **67**, 757 (1991); *Phys. Rev. B* **49**, 7904 (1993); *ibid.* **50**, 14016 (1994); *ibid.* **54**, 1584 (1996).
- ³ A. Schiller and K. Ingersent, *Phys. Rev. Lett.* **75**, 113 (1995); G. Zaránd, D.L. Cox, and A. Schiller, *Phys. Rev. B* **62**, R16227 (2000).
- ⁴ M.H. Hettler, A.N. Tahvildar-Zadeh, M. Jarrell, T. Pruschke, H.R. Krishnamurthy, *Phys. Rev. B* **58**, R7475 (1998); M.H. Hettler, M. Mukherjee, M. Jarrell, and H. R. Krishnamurthy *Phys. Rev. B* **61**, 12739 (2000).
- ⁵ S. Biermann, A. Georges, A. Lichtenstein, and T. Giamarchi, *Phys. Rev. Lett.* **87**, 276405 (2001).
- ⁶ G. Kotliar, S. Savrasov, G. Palsson, and G. Biroli, *Phys. Rev. Lett.* **87**, 186401 (2001) and the references therein.
- ⁷ G. Biroli and G. Kotliar, *Phys. Rev. B* **65**, 155112 (2002).
- ⁸ S. Sachdev and J. Ye, *Phys. Rev. Lett.* **70**, 3339 (1993).
- ⁹ H. Kajueter, Ph.D. thesis, Rutgers University (1996).
- ¹⁰ Q. Si, S. Rabello, K. Ingersent, and J.L. Smith, *Nature* **413** 804 (2001); J.L. Smith and Q. Si, *Phys. Rev. B* **61**, 5184 (2000); Q. Si and J.L. Smith, *Phys. Rev. Lett.* **77**, 3391 (1996).
- ¹¹ O. Parcollet and A. Georges, *Phys. Rev. B* **59**, 5341 (1999).
- ¹² R. Chitra and G. Kotliar, *Phys. Rev. Lett.* **84**, 3678 (2000); *Phys. Rev. B* **63**, 115110 (2001).
- ¹³ Y. Motome and G. Kotliar *Phys. Rev. B* **62**, 12800 (2000).

- ¹⁴ S. Pankov, G. Kotliar, and Y. Motome, cond-mat/0112083.
- ¹⁵ V.I. Anisimov, A.I. Poteryaev, M.A. Korotin, A.O. Anokhin, and G. Kotliar, *J. Phys.: Condens. Matt.* **9**, 7359 (1997).
- ¹⁶ S. Savrasov, G. Kotliar, and E. Abrahams, *Nature* **410**, 793 (2001); S. Savrasov and G. Kotliar, *Phys. Rev. Lett.* **84**, 3670 (2000).
- ¹⁷ G. Kotliar and S.Y. Savrasov, *Model Hamiltonians and First Principles Electronic Structure Calculations in New Theoretical Approaches to Strongly Correlated Systems*, Ed. A.M. Tsvelik, Kluwer Academic Publishers (2001).
- ¹⁸ For a review, see K. Held, I.A. Nekrasov, G. Keller, V. Eyert, N. Blümer, A.K. McMahan, R.T. Scalettar, T. Pruschke, V.I. Anisimov, and D. Vollhardt, in *Quantum Simulations of Complex Many-Body Systems: From Theory to Algorithms*, Ed. J. Grotendorst, D. Marx, and A. Muramatsu, NIC Series Vol. 10 (NIC Directors, Forschungszentrum Jülich, 2002), p. 175.
- ¹⁹ J.E. Hirsch, *Phys. Rev. Lett.* **87**, 206402 (2001).
- ²⁰ M. Springer and F. Aryasetiawan, *Phys. Rev. B* **57**, 4364 (2001).
- ²¹ N.E. Zein and V.P. Antropov, cond-mat/0202483.
- ²² G.D. Mahan, *Many-Particle Physics*, Plenum Press (1981), Chapter 5.
- ²³ D.R. Hamann and S.B. Fahy, *Phys. Rev. B* **47**, 1717 (1993).
- ²⁴ Lars Hedin, *Phys. Rev.* **139** A796 (1965).
- ²⁵ R. Pietig, R. Bulla, and S. Blawid *Phys. Rev. Lett.* **82**, 4046 (1999).
- ²⁶ A. Ochiai, T. Suzuki, and T. Kasuya, *J. Phys. Soc. Jpn.* **59**, 4129 (1990).
- ²⁷ S. Mori, C.H. Chen, and S.-W. Cheong, *Nature (London)* **392**, 473 (1998); C.H. Chen and S.-W. Cheong, *Phys. Rev. Lett.* **76**, 4042 (1996).

- ²⁸ Tomioka, A. Asamitsu, H. Kuwahara, and Y. Tokurai, *J. Phys. Soc. Jpn.* **66**, 302 (1997).
- ²⁹ J.B. Torrance, J.E. Vazquez, J.J. Mayerle, and V.Y. Lee, *Phys. Rev. Lett.* **46**, 253 (1981);
J. B. Torrance, A. Girlando, J. J. Mayerle, J. I. Crowley, V. Y. Lee, and P. Batail, *ibid.* **47**, 1747 (1981).
- ³⁰ N. Nagaosa and J. Takimoto, *J. Phys. Soc. Jpn.* **55**, 2735 (1986).
- ³¹ T. Egami, S. Ishihara, and M. Tachiki, *Science* **261**, 1307 (1993); S. Ishihara, T. Egami, and M. Tachiki, *Phys. Rev. B* **49**, 8944 (1994); S. Ishihara, M. Tachiki, and T. Egami, *ibid.* **49**, 16123 (1994).
- ³² In E-DMFT, since the on-site interaction U does not get renormalized, one may find that the procedure of separating the Hartree contribution does not affect the result as far as the local interaction is concerned. So practically one can leave this term alone. The difference comes from the non-local interaction where the bare interaction vertex is replaced by an effective, on-site, and retarded one.
- ³³ C.J. Bolech, S.S. Kancharla, and G. Kotliar, Preprint.
- ³⁴ J.W. Negele and H. Orland, *Quantum Many-Particle Systems*, Addison-Wesley (1988), Chapter 2.
- ³⁵ J.E. Hirsch and R.M. Fye, *Phys. Rev. Lett.* **56**, 2521 (1986).
- ³⁶ G.M. Buendia, *Phys. Rev. B* **33**, 3519 (1986).
- ³⁷ The overall accuracy of the E-DMFT, which consists of the QMC solution of the impurity model and the self-consistent calculations, is of the order 0.001. If not otherwise specified, *all* the data presented in this paper have the accuracy ~ 0.001 . The centers of the various symbols in the diagrams represent the locations of the data while their sizes do *not* reflect the accuracy. All the functions of the Matsubara frequency are calculated at the corresponding discrete values. The lines connecting the points are guides to the eye.

- ³⁸ In presenting the phonon related results we *always* set $\lambda = 0$. A finite λ is used *only* in the QMC simulations.
- ³⁹ S. Doniach and E.H. Sondheimer, *Green's Functions for Solid State Physicists*, Benjamin (1974), Chapters 6 and 7.
- ⁴⁰ G. Strinati, H.J. Mattausch, and W. Hanke, Phys. Rev. Lett. **45**, 290 (1980); Phys. Rev. **B 25**, 2867 (1982).
- ⁴¹ B. Holm and U. von Barth, Phys. Rev. B **57** 2108 (1998).
- ⁴² C.-O. Almbladh, U. Von Barth, and R. Van Leeuwen, Int. J. Mod. Phys. B **13**, 535 (1999).
- ⁴³ A.A. Abrikosov, L.P. Gorkov, I.E. Dzyaloshinski, *Methods of Quantum Field Theory in Statistical Physics*, Prentice-Hall (1963), Section 10.
- ⁴⁴ P. Nozieres, *Theory of Interacting Fermi Systems*, Addison-Wesley (1964), Chapter 3.
- ⁴⁵ W. Metzner and D. Vollhardt, Phys. Rev. Lett. **62**, 324 (1989).
- ⁴⁶ L. Steinbeck, A. Rubio, L. Reining, M. Torrent, I.D. White, and R.W. Godby, Comput. Phys. Commun. **125**, 105 (2000); T.J. Pollehn, A. Schindlmayr, and R.W. Godby, J. Phys.: Cond. Matt. **10**, 1273 (1998).
- ⁴⁷ S.S. Kancharla and C.J. Bolech, Phys. Rev. B **64**, 85119 (2001).
- ⁴⁸ We would like to thank Dr. S. S. Kancharla and Dr. C. J. Bolech for allowing us to use their DMRG programs for the calculation.
- ⁴⁹ M.E. Torio, A.A. Aligia, and H.A. Ceccatto Phys. Rev. B **64**, R121105 (2001) and the references therein.

FIGURES

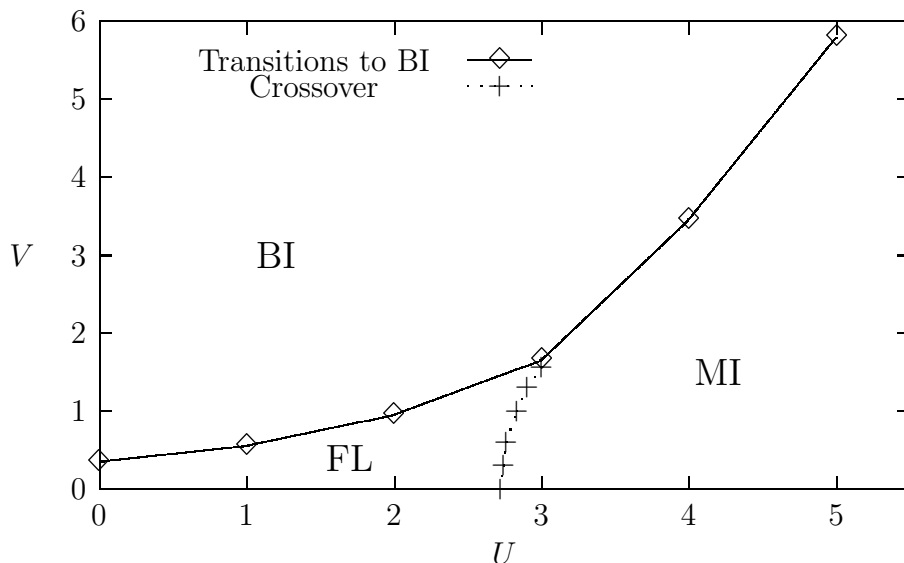


FIG. 1. The phase diagram of the 3D U-V model at $\beta = 5.0$. The centers of the symbols represent the numerical results whose accuracy is of the order of 0.01. The line bounded the BI phase represents the phase transitions from the FL and MI phases. The phase transition line is found by approaching the instability of the E-DMFT iteration from the smaller values of V . The line in between the FL and MI phases represents a crossover. It is determined by the values of U and V at which $\text{Im} G_{\sigma}(ip_0) = -0.5$.

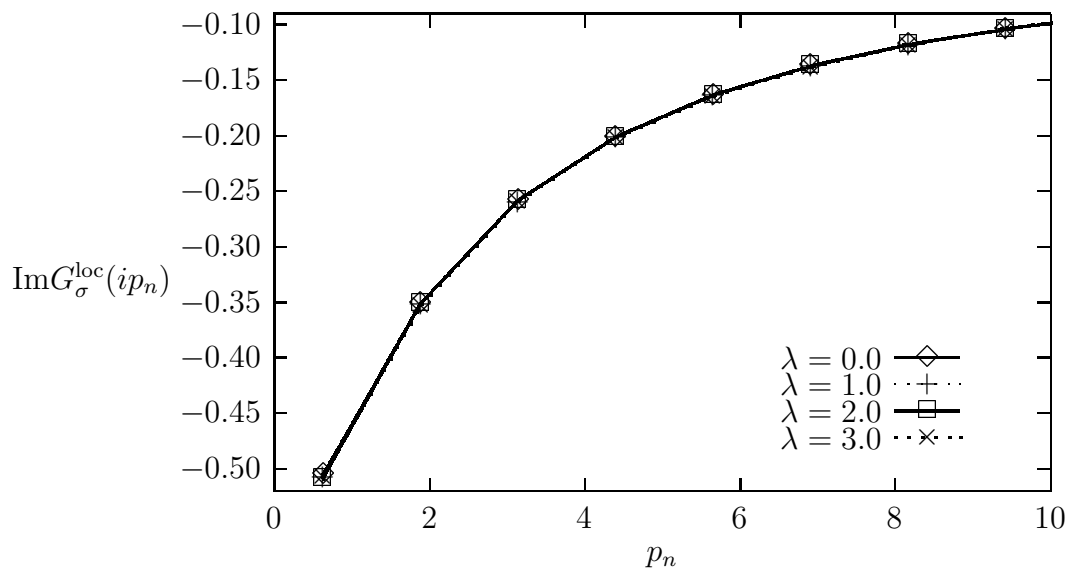


FIG. 2. The imaginary part of the electron Green's function at four different values of λ calculated at $U = 3.0$ and $V = 1.6$ as a function of the Matsubara frequency³⁷.

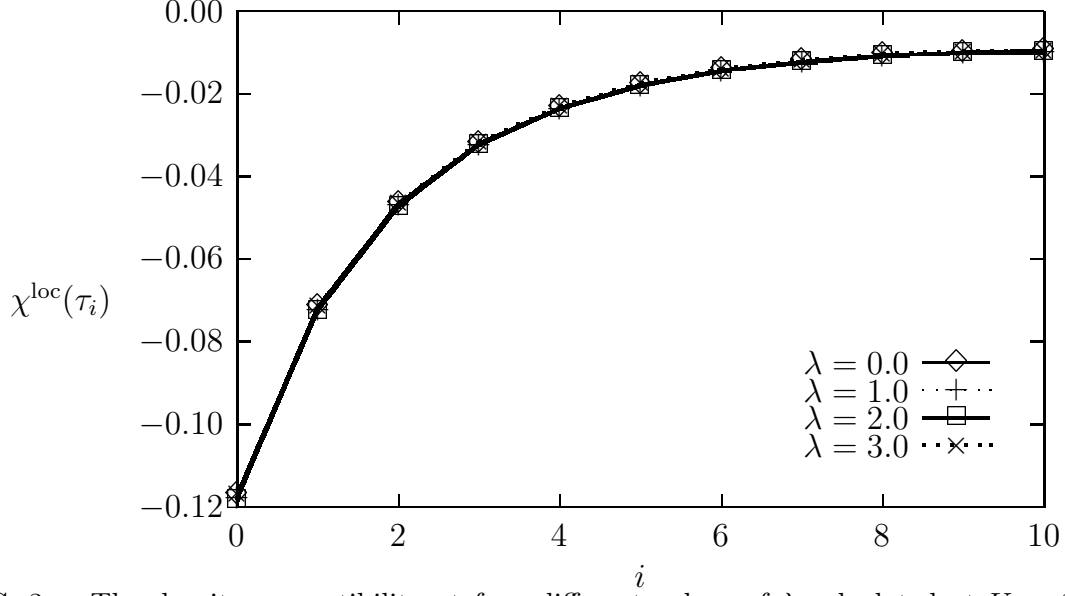


FIG. 3. The density susceptibility at four different values of λ calculated at $U = 3.0$ and $V = 1.6$ as a function of the imaginary time.

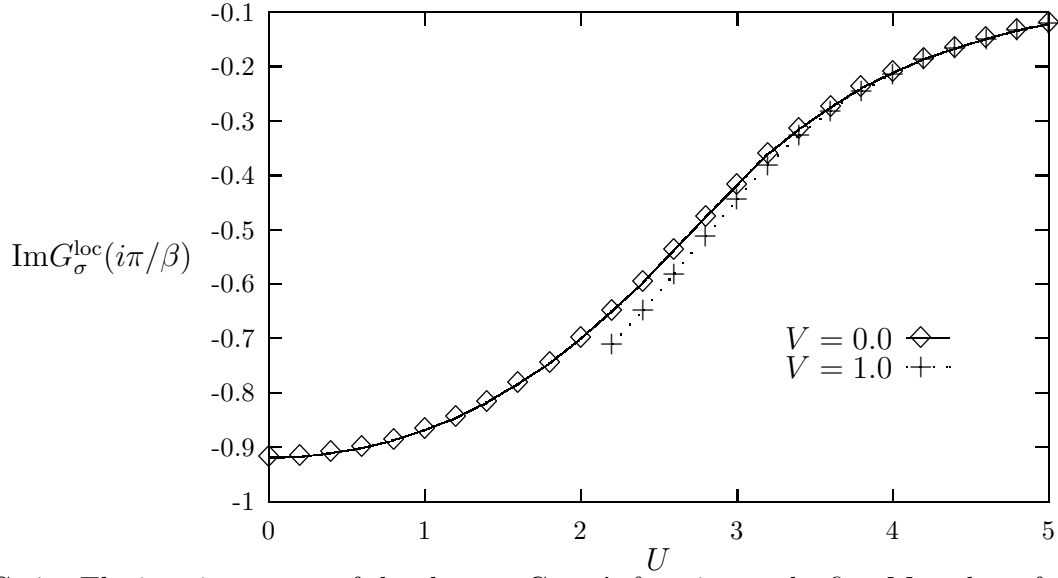


FIG. 4. The imaginary part of the electron Green's function at the first Matsubara frequency, $\text{Im} G_{\sigma}^{\text{loc}}(i\pi/\beta)$, as a function of the on-site interaction U for two different values of V .

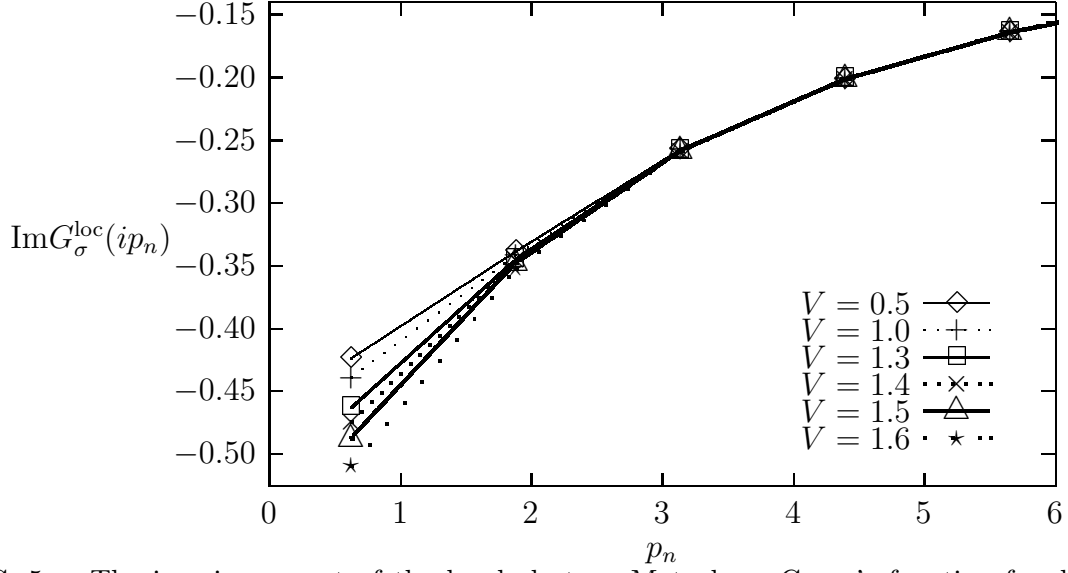


FIG. 5. The imaginary part of the local electron Matsubara Green's function for different values of the interaction V at fixed $U = 3.0$.

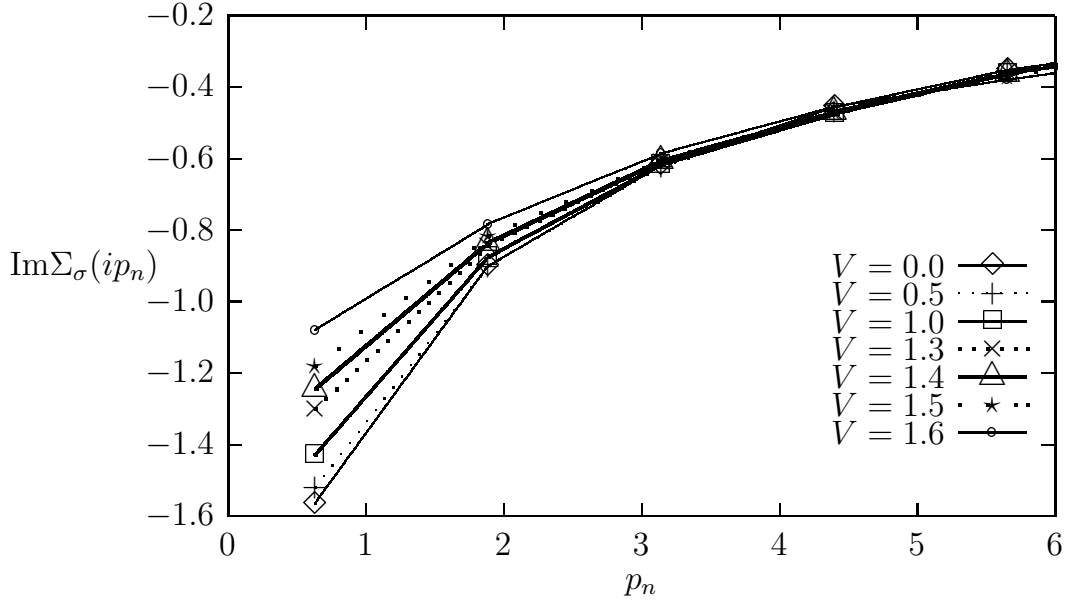


FIG. 6. The frequency dependence of the imaginary part of the electron self-energy $\Sigma_\sigma(ip_n)$ at different values of the interaction V at fixed $U = 3.0$.

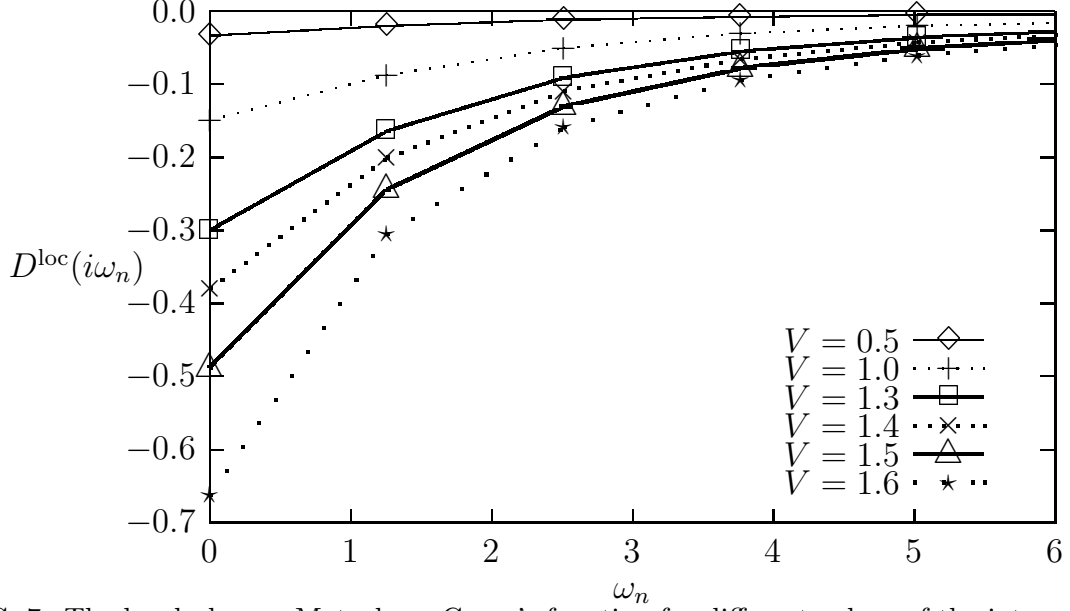


FIG. 7. The local phonon Matsubara Green's function for different values of the interaction V at fixed $U = 3.0^{38}$.

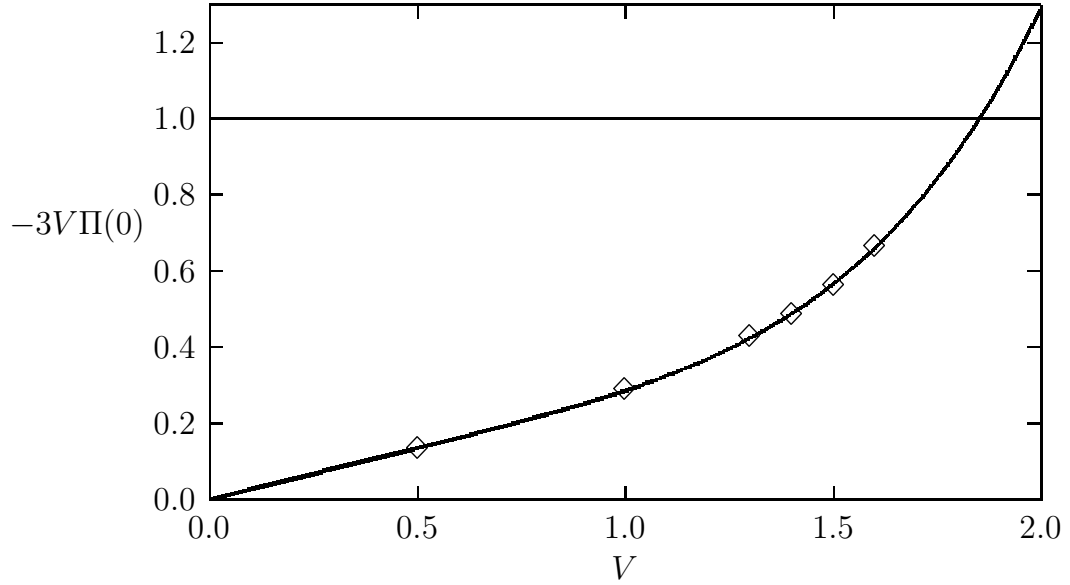


FIG. 8. The rescaled phonon self-energy at the most unstable point with $k = (\pi, \pi, \pi)$ and $\omega_n = 0$ for $U = 3.0$. The diamonds represent the calculated data. The curve is plotted using a polynomial fitting of the phonon self-energy Π (which is even in V) up to V^4 . From the extrapolation the transition is at $V_c \simeq 1.85$. This value is less accurate than the one from QMC due to the non-analyticity near the transition.

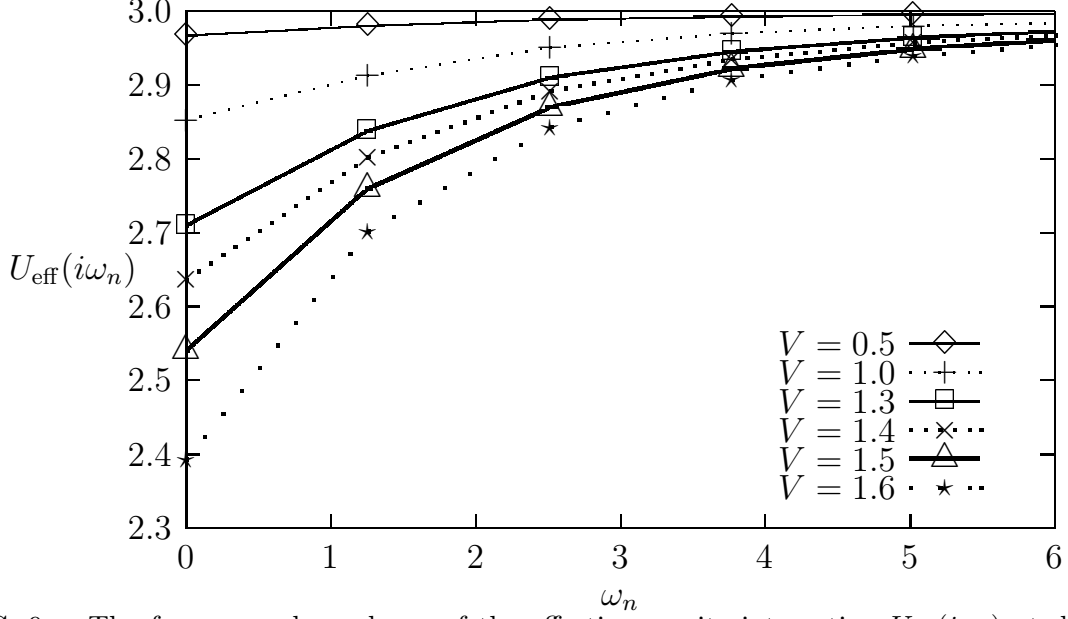


FIG. 9. The frequency dependence of the effective on-site interaction $U_{\text{eff}}(i\omega_n)$ at different values of the interaction V at fixed $U = 3.0$.

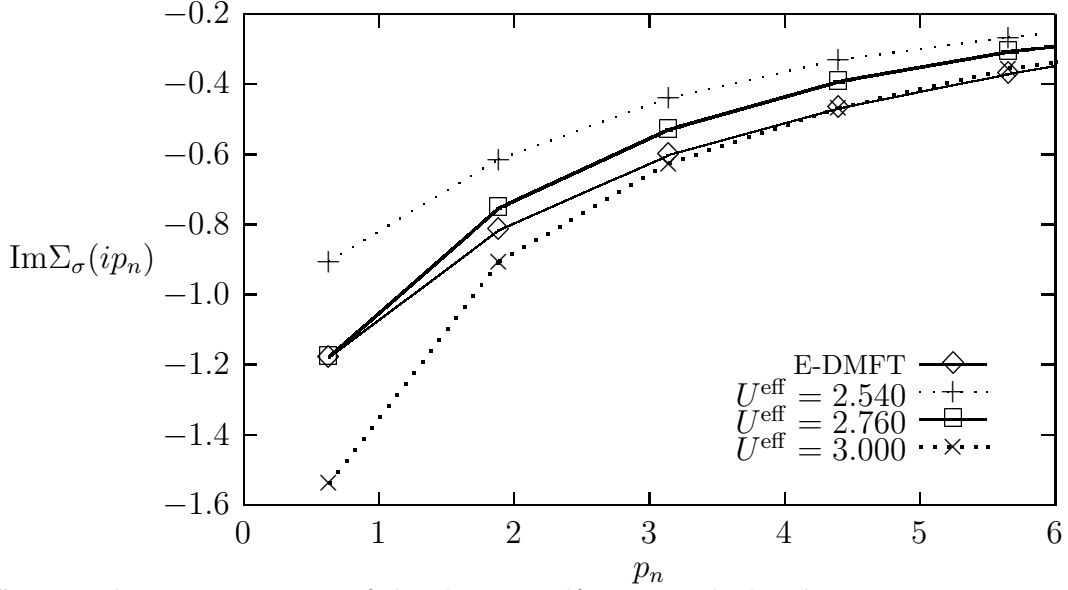


FIG. 10. The imaginary part of the electron self-energy calculated using E-DMFT at $U = 3.0$ and $V = 1.5$ and at the corresponding $U^{\text{eff}} = U_{\text{eff}}(i\omega_n)$ for $n = 0, 1, \infty$ with $V = 0$. We used $U_{\text{eff}}(i\omega_0) = 2.540$ and $U_{\text{eff}}(i\omega_1) = 2.760$ from our E-DMFT calculation. Obviously $U_{\text{eff}}(i\omega_\infty) = 3.0$

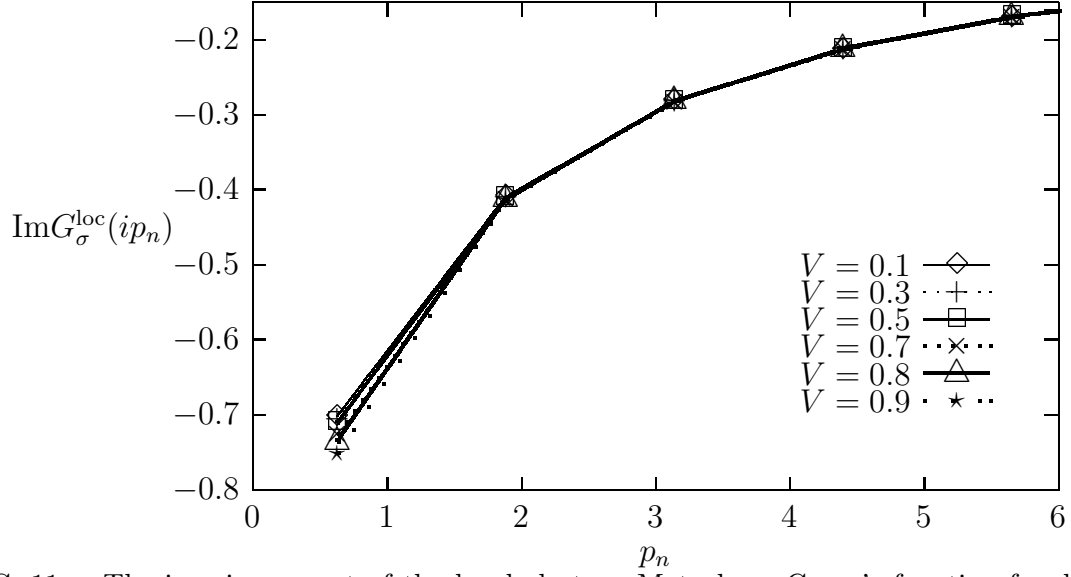


FIG. 11. The imaginary part of the local electron Matsubara Green's function for different values of the interaction V at fixed $U = 2.0$.

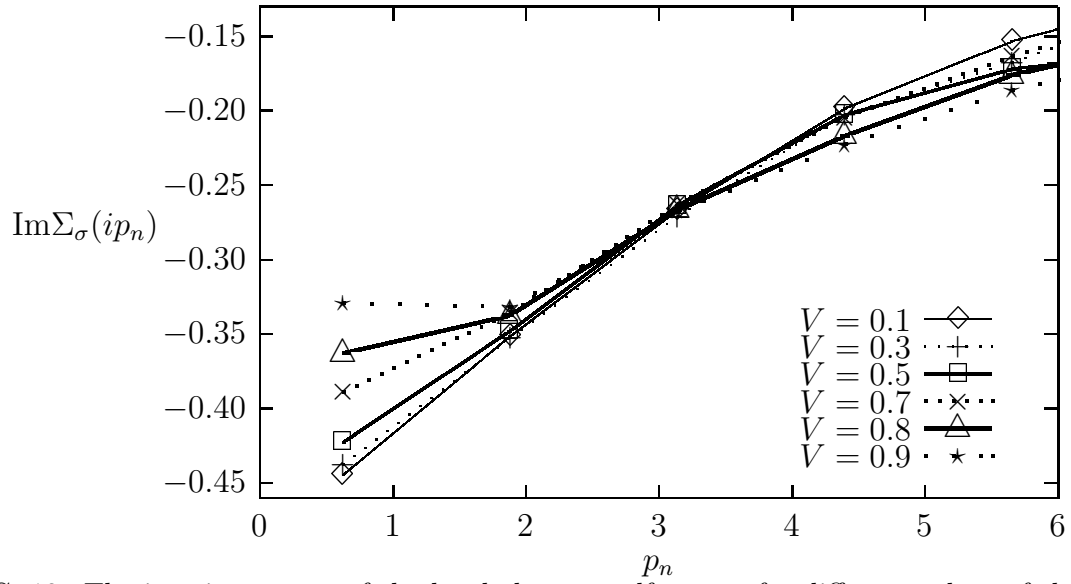


FIG. 12. The imaginary part of the local electron self-energy for different values of the interaction V at fixed $U = 2.0$.

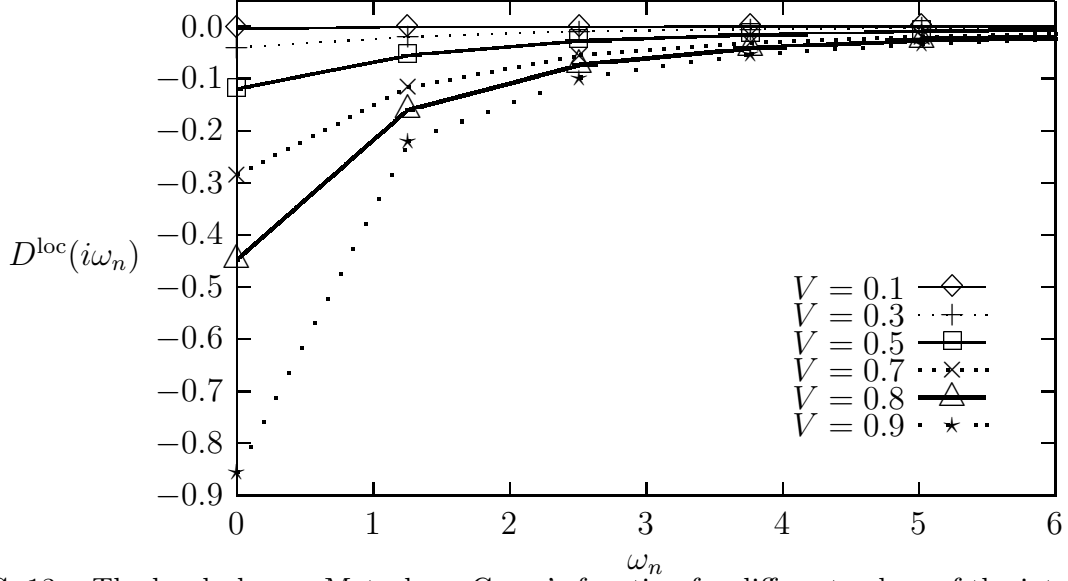


FIG. 13. The local phonon Matsubara Green's function for different values of the interaction V at fixed $U = 2.0$.

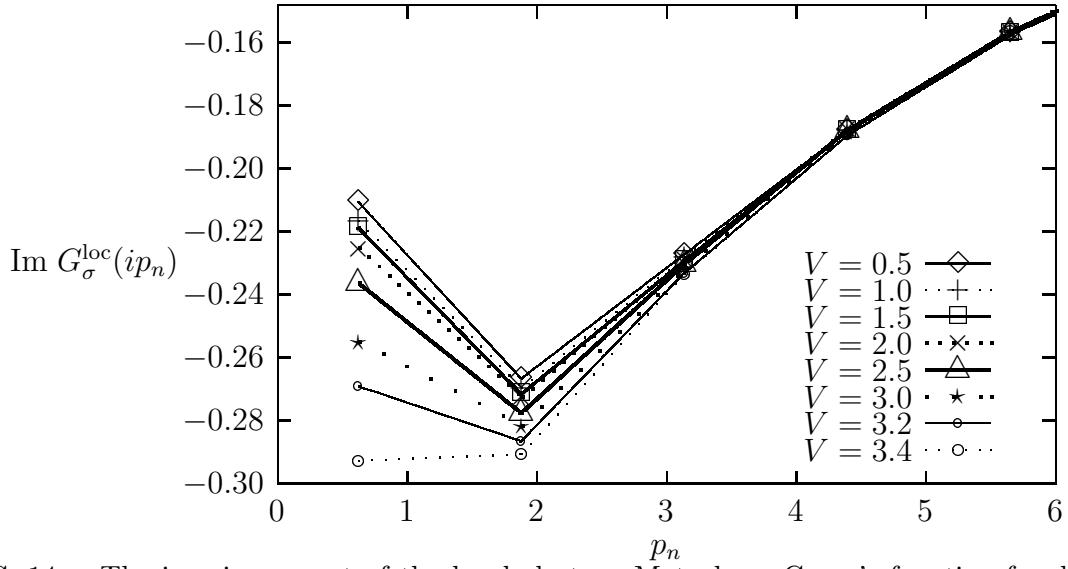


FIG. 14. The imaginary part of the local electron Matsubara Green's function for different values of the interaction V at fixed $U = 4.0$.

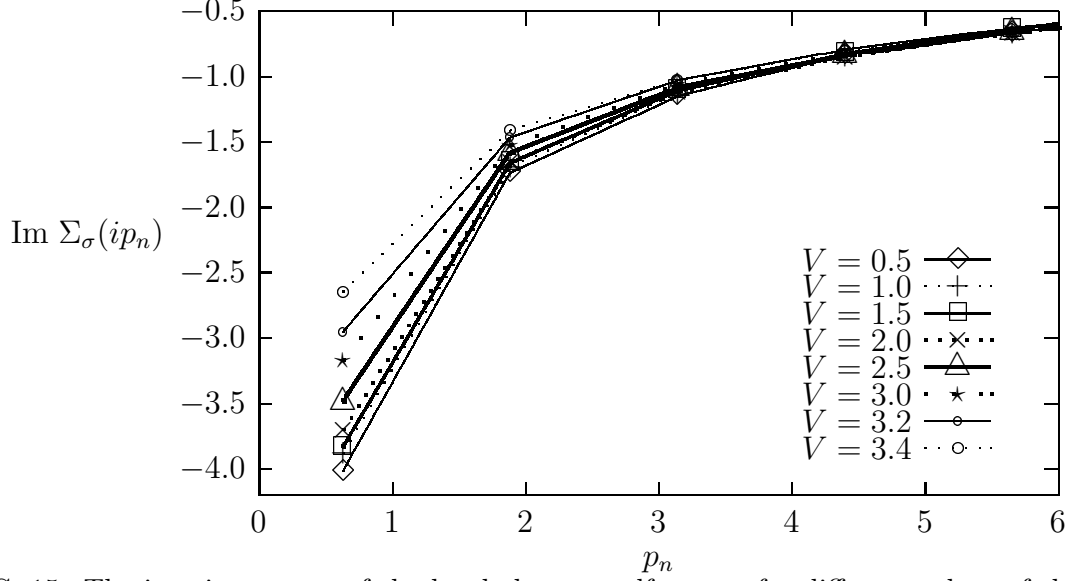


FIG. 15. The imaginary part of the local electron self-energy for different values of the interaction V at fixed $U = 4.0$.

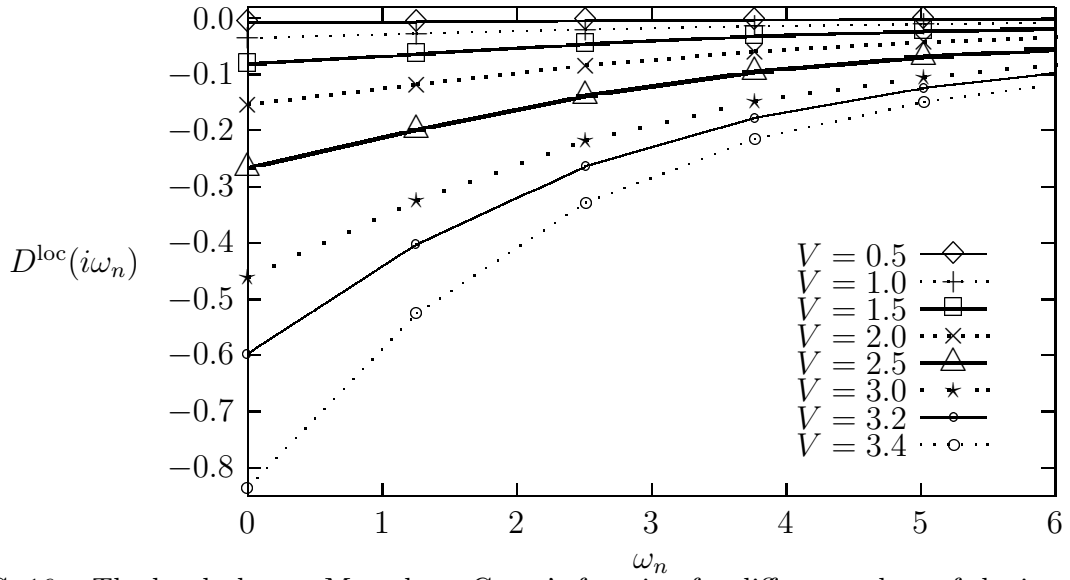
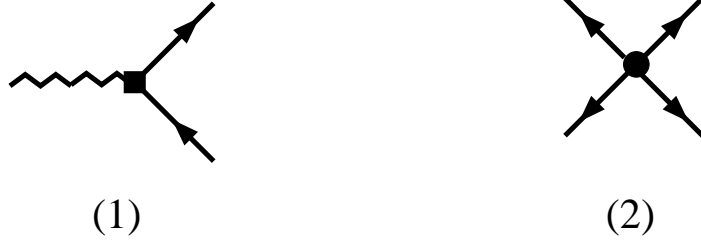


FIG. 16. The local phonon Matsubara Green's function for different values of the interaction V at fixed $U = 4.0$.

$$\Phi^{E\text{-DMFT-GW}}[G, D] = \underset{i \neq j}{\text{O} \text{---} \text{O}} + \underset{i \neq j}{\text{O} \text{---} \text{O}} + \sum_i \Phi[G_{ii}, D_{ii}]$$

FIG. 17. The 2-particle irreducible functional $\Phi[G, D]$ in the E-DMFT-GW approach.

A. Interaction Vertices



B. Generalized GW Self-Energies at $i \neq j$

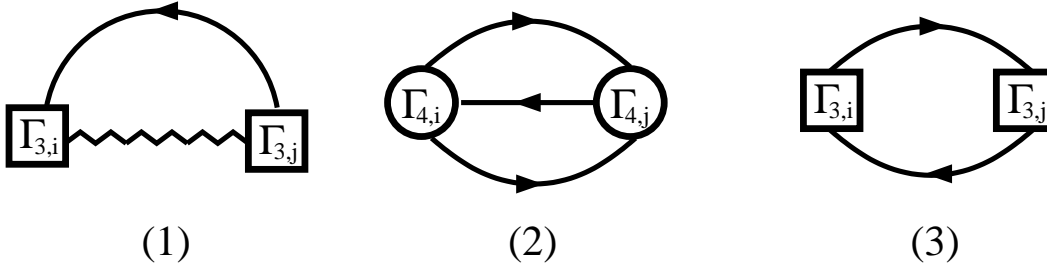


FIG. 18. A. The bare interaction vertices contained in Eqs.(6) and (34), that is, the local electron-phonon interaction A(1) and the local Hubbard interaction A(2). B. The non-local self-energy contributions described in Eq.(49) [B(1) and B(2)] for electrons and Eq.(50) [B(3)] for phonons. The strengths of the leading contributions (from the nearest neighbors) for the three diagrams are $O[V/d]$, $O[U^2/d^{3/2}]$, and $O[1/d]$, respectively. Since in each of the diagrams we require the vertices be from different lattice sites, there is no double counting.

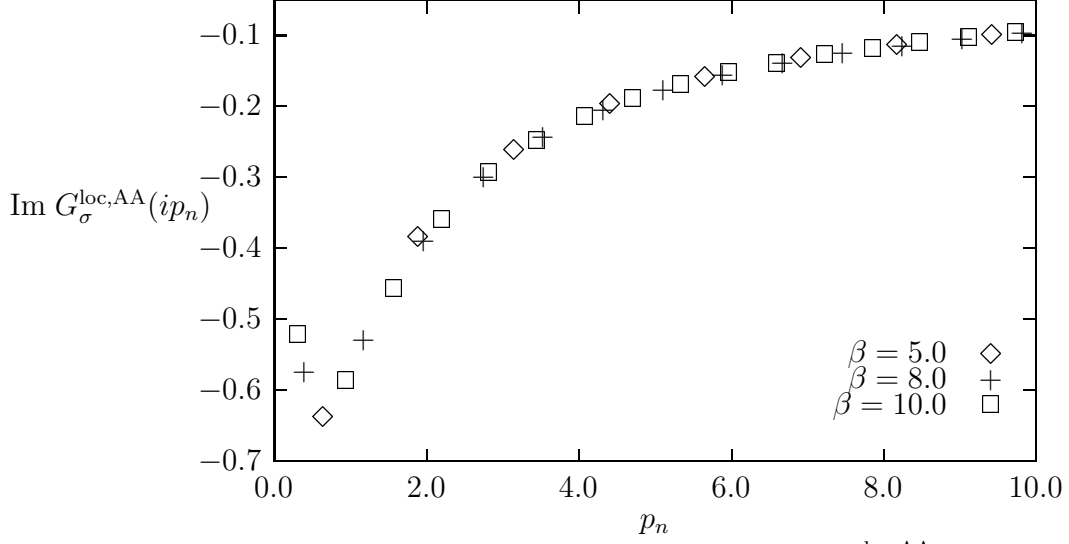


FIG. 19. The imaginary part of the local electron Green's function $G_{\sigma}^{\text{loc,AA}}(ip_n)$ at $U = 5.0$, $V = 0.5$, and $\mu = 2.0$. The results at three different inverse temperatures are shown³⁸. Within the accuracy of the calculation, the three sets of data lie on a smooth curve which means the thermal effects on the result has already been suppressed due to the band gap.

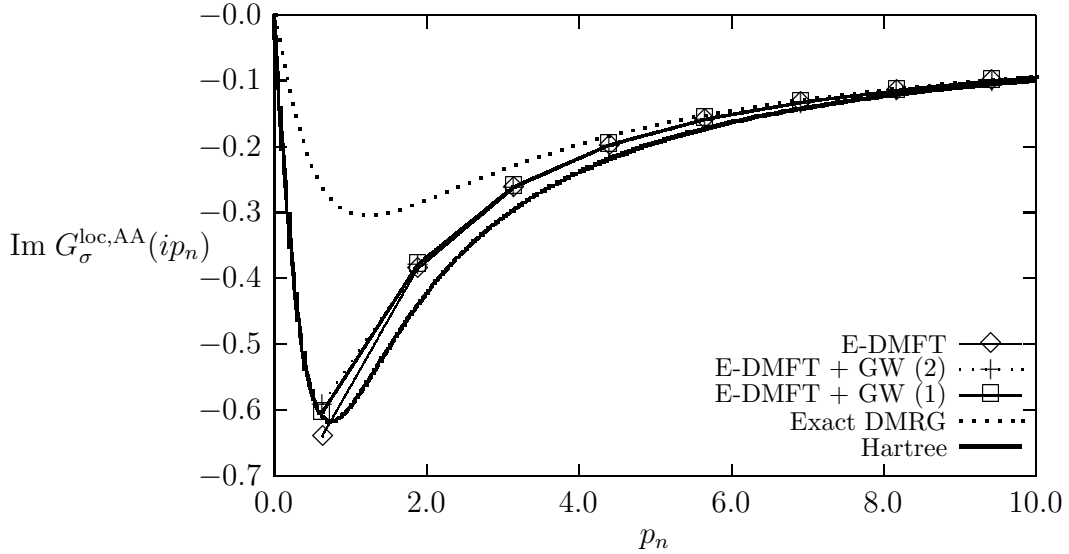


FIG. 20. The imaginary part of the local electron Green's function $G_{\sigma}^{\text{loc,AA}}(ip_n)$ at $U = 5.0$, $V = 0.5$, $\mu = 2.0$, and $\beta = 5.0$. The data labeled as GW(1) comes from the contribution described by Fig.18B(1) and GW(2) from Fig.18B(2). It can be seen that GW(1) and GW(2) makes corrections at the same order to the E-DMFT result.

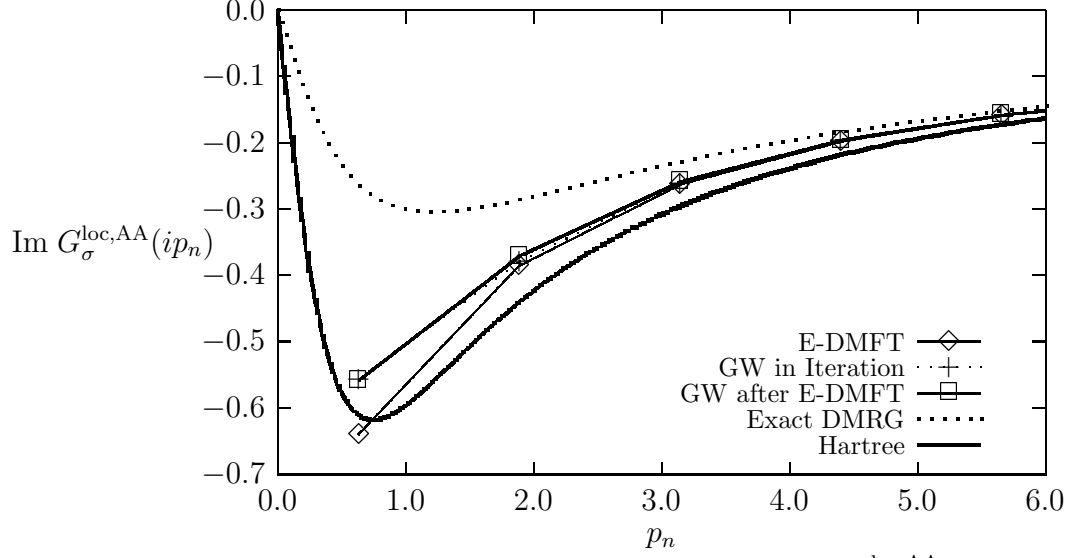


FIG. 21. The imaginary part of the local electron Green's function $G_{\sigma}^{\text{loc,AA}}(ip_n)$ at $U = 5.0$, $V = 0.5$, $\mu = 2.0$, and $\beta = 5.0$.

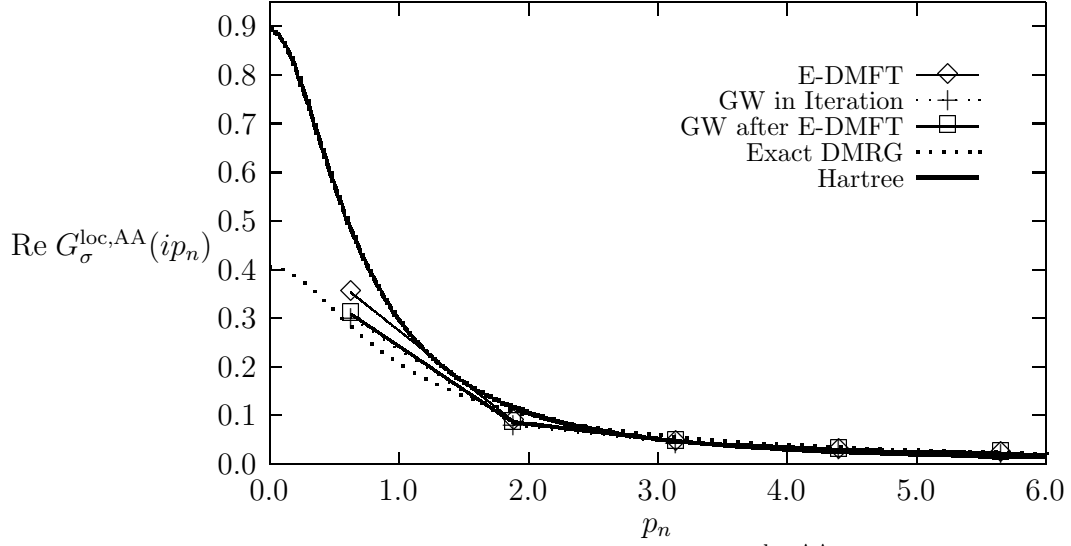


FIG. 22. The real part of the local electron Green's function $G_{\sigma}^{\text{loc,AA}}(ip_n)$ at $U = 5.0$, $V = 0.5$, $\mu = 2.0$, and $\beta = 5.0$.

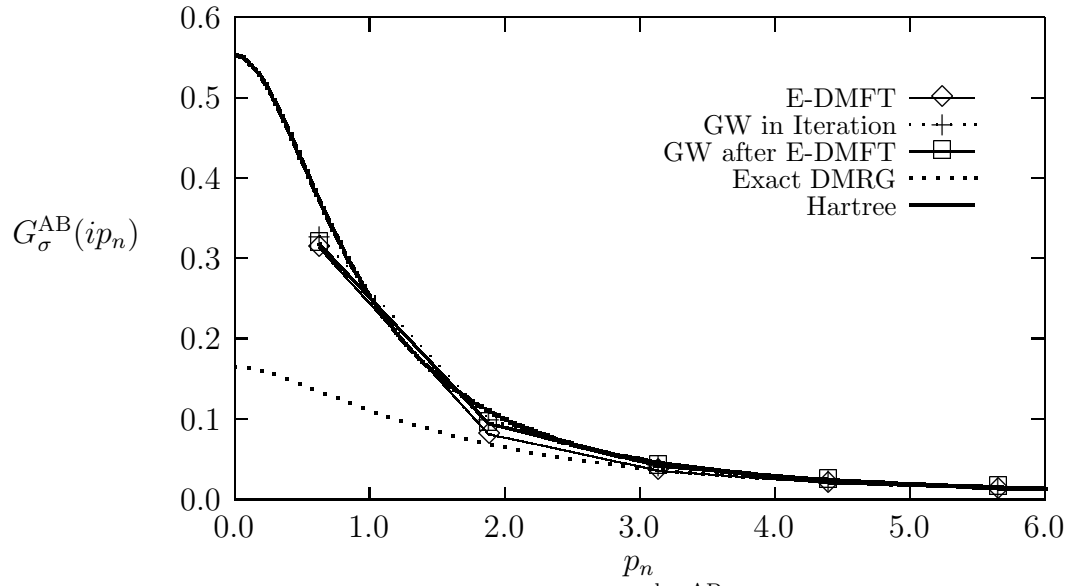


FIG. 23. The off-diagonal electron Green's function $G_{\sigma}^{\text{loc,AB}}(ip_n)$ at $U = 5.0$, $V = 0.5$, $\mu = 2.0$, and $\beta = 5.0$.